UNIVERSITÉ ABDOU MOUMOUNI

----0----0----0-----

MASTER RESEARCH PROGRAM

Climate Change and Energy

A thesis submitted in partial fulfillment

For the degree of Master of Science in

Climate change and energy

SIMULATING THE IMPACT OF CLIMATE CHANGE ON SOLAR ENERGY POTENTIAL OVER WEST AFRICA: THE CASE OF MALI

Fatoumata DIALLO

Defense: 07-03-2018
Academic year: 2017-2018
Niamey, Niger

Supervisor: Dr. Benjamin LAMPTEY.
Co-Supervisor: Dr. Souleymane SANOGO

ACKNOWLEDGEMENTS

All the praises and thanks be to Allah, the almighty for giving me inspiration, patience, time and strength to finish this work.

First and foremost, I acknowledge with thanks the scholarship and financial support provided to me by BMBF, the Federal Ministry of Education and Research of Germany and the West African Science Service Centre on Climate Change and Adapted Land Use (WASCAL). The study is part of the Scholarship Programme, sponsored by German Federal Ministry of Education and Research, the West Africa Science Service Center on Climate Change and Land Use (WASCAL). The study was supervised by Dr. Benjamin LAMPTEY and Dr. Souleymane SANOGO.

I am heartily thankful to my two Supervisors Dr. Benjamin LAMPTEY and Dr. Souleymane SANOGO. I would like to thank the Director of MRP-CCE Dr. Rabani ADAMOU, the Coordinator of MRP-CCE, Dr.INOUSSA Maman Maarouhi and all the staff of the MRP Climate change and energy for all their time and contribution for the success of this project.

I would like to show my gratitude to my mother Aissata BA, my sisters Fatoumata DIALLO, Fatoumata HAIDARA, Aminata DIALLO, Aissata DIALLO and my Brother AMADOU DIALLO for supporting me throughout my life. They always encourage me even though they missed me a lot during my studies.

The greatest honor is for my father Oumar DIALLO who put me on the right track to achieve the destiny.

I would moreover like to express my gratitude to all the people of the Laboratory of optic spectroscopy and atmospheric sciences (LOSSA) in the Faculty of sciences and technics of Bamako (FST), and also Abdoulaye BALLO and Adama SAMAKE for their help for obtaining my data during my field work.

Finally, I thank everyone who has contributed to this study in one way or the other. Especially, I present my thanks to all the MRP students in Climate Change and Energy. Last two years have been quite an experience for me and you have all made it a memorable time in my life.

Table des matières

LIST OF TABLES, MAPS AND FIGURES

List of Tables:

AR5	Fifth Assessment Report
CMIP5	Coupled Model Inter-Comparison Phase 5
CEMG	Clean Energy Mini-Grid
CO_2	Carbon dioxide
ECOWAS	Economic Commission of West African States
EIA	Energy Impact Assessment
GHGs	Greenhouse Gases
GCMs	Global Climate Model
GW	Gigawatts
IPCC	Intergovernmental Panel for Climate Change
IRENA	International Renewable Energy Agency
KW	kilowatts
MW	Megawatts
MRP-CCE	Master Research Program Wascal Climate Change and Energy
PV	Photovoltaics
RCP	Representative Concentration Pathways
RE	Renewable Energy
REN21	Renewable Energy Policy Network for the 21st Century
RCMs	Regional Climate Model
REA	Renewable Energy for Africa
swddir	Shortwave surface downward direct irradiance
swddif	Shortwave surface downward diffuse irradiance
ts	Surface Temperature
WRF	Weather Research and Forecasting
WASCAL	West African Science Service Centre on Climate Change and Adapted Land Use
TFEC	Total Final Energy Consumption

Abstract

Solar energy remains one of the few bright spots in renewable energies in the 21 st century. Solar farms can provide clean renewable energy to homes, businesses, and the agricultural sector.
An investigation was done on the impact of climate change on the solar energy potential in two locations in the Sahelian part of Mali (Bamako and Mopti) together with an assessment of the suitability of these regions for siting solar energy panels for both present day and future climate.

The study was done using the output of the 12-km spatial resolution weather research and forecasting (WRF) model. The results showed that the increase in Shortwave-Surface-Downward-Diffuse-Irradiance (*swddif)* is more significant in the near and far future in Bamako than Mopti. For the near future an increase of +2.2W/m^2 for Bamako and +1W/m^2 for Mopti were observed in May. For the far future, an increase of +3.5W/m^2 for Bamako and +1.75W/m^2 for Mopti were observed in May. However, increase in Shortwave-Surface-Downward-Direct-Irradiance *(swddir*) is almost the same for Bamako and Mopti for the near future an increase of +2W/m^2 observed in the month of July for both Bamako and Mopti and for the far future an increase of +6W/m^2 observed in the month of July for both Bamako and Mopti. There is an increase of temperature over both localities and it's more significant in Mopti than Bamako. A continuous increase in surface temperature(*ts*) is clearly observed for the near and far future over both Bamako and Mopti. The peaks over both localities are observed in May, September, October, and November. A high augmentation is observed during the month of February for both near and far future. Thus, based on the three parameters used in this study, the locality of Mopti will be more suitable for solar energy panels to satisfy the energy needs in Mali.

Key Words: Solar energy, Climate change, WRF, *swddi*r, *swddif, ts.*

Chapter 1

INTRODUCTION

1.1. Background

The effects of climate change can be seen everywhere across the world (e.g. increase in droughts, floods, intense storms, among others, arguably can be attributed to climate change). Extreme weather patterns have a huge impact on the environment, economy and human well-being. The emissions of greenhouse gases (GHGs) is mainly due to increase in anthropogenic greenhouse gas (GHG) concentrations (IPCC, 2007). The consumption of fossil fuels is the main source of emissions of global anthropogenic GHG emissions mainly from electricity production (IPCC, 2011).

Energy from the sun is the fundamental source of energy driving our climate system. Changes in the total amount of energy received at the earth surface, can lead to climate change at global, regional, and local scales (POWER et al., 2005). Energy is the driver of the development in countries all over the world. It contributes to the sustainable development of nations. Access to electricity is low in many countries in the world and populations are relying on wood, charcoal or biomass materials to satisfy their energy needs. The growth in population leads to an increase in the energy demand which in turn leads to changes in the climate. In order not to compromise future energy generation, there is a need to use renewable energy (RE) such as (solar energy, wind energy, and biomass). This REs have high potential in many countries in the world. Solar energy is the cleanest source of energy (IREN21, 2011). According to Martin et al. (2016), there has been considerable effort to make use of solar energy efficiently since the industrial revolution. This effort has been made in anticipation that fossil fuels would run out in the future. However, very few resources have been directed towards forecasting incoming energy at ground level. It is necessary for the integration of solar energy (thermal power and photovoltaic) into electric grid within different sources of electric power generation, to have energy forecasting models. These

models will become more complex as they gain recognition as an energetic resource in the near future. Photovoltaic and solar thermoelectric power are main sources of solar energy for electricity generation. There is a need for necessary information on solar radiation to predict the amount of energy which will be produced.

Studies have indicated that, knowing and understanding the trends and variability of past climate is fundamental to understanding the climate system and can help mitigate the damages from climate change (e.g. Moore et al., 2001; Luhunga et al., 2016**)**. Nowadays, Global Climate Models (GCMs) are available for simulating the response of the global climate system to increased greenhouse gas concentrations in the atmosphere (e.g. Villegas and Jarvis 2010; Daniels et al.,2012; Hassan et al., 2013; Xiaoduo et al., 2012). However, the spatial resolution of the GCMs are too coarse for impact studies as impact and adaptation studies require simulation data with high spatial resolution. Thus, there is the need to downscale the GCMs for this purpose. The use of Regional Climate Models (RCMs) to downscale GCMs, is the widely applied method to obtain high resolution climate information (Denis et al., 2002; Min et al., 2013). RCMs have been used over large domains to provide climate simulation with high resolution. Some studies indicate the sensitivity of RCM simulations to surface forcing as well as the size of the integration domain (e.g. Xiaoduo et al., 2012, Roux 2009, Wilby and Fowler 2011). The model performance is not homogenous across regions. For instance, Endris et al., 2013, demonstrated that RCMs simulated rainfall better in one region but more poorly in another region over the same time period. In another study, the Rossby Centre Atmospheric model version 3 (RCA3) RCM simulated annual mean precipitation and the mean seasonal cycle of precipitation much better when driven by ECHAM5 than ECHAM4. ECHAM4 and ECHAM5 driven simulations overestimated both the mean sea level pressure and sea level pressure gradient, while HadCM3 driven simulations underestimated both of these features (Min et al., 2013; Meier et al.,2011).

With regards to radiation, many radiation related studies in the Northern Hemisphere have been based on the evaluation of the trends and variability in global radiation and a few studies have analyzed the variability in the diffuse and direct components of solar radiation (Power et al., 2005).

1.2. Problem statement

The main source of electricity production in Mali are, hydropower and fossil fuel. The heavy dependence on imported petroleum is putting the country's foreign reserves under pressure and highlighting the need for the development of the energy sector. Mali has a huge potential of renewable energy (wind, Biomass, Solar) that could be harnessed to satisfy the country's energy needs. Given the current trend of changes in climate, it is important to understand the impact of climate variability and change on renewable energy resources. With regards to hydropower generation, it is common knowledge that river flow in the country has changed dramatically and this change is hypothesized to be due to climate change. As stated earlier concerning radiation related studies in the Northern Hemisphere, few studies have analyzed the variability in the diffuse and direct components of solar radiation but understanding the variability of these parameters is critical for the integration of solar energy into the national electric grid. Thus, there is a need for high resolution climate simulations if meaningful studies on the impact of climate variability and change are to be carried out at the national level. So far, no study has been carried out on the assessment of the impact of climate change on solar energy potential in the country. However, (Badger et al., 2012) only estimated wind and solar resources in the country by using Satellite data.

1.2.1. Objectives of the thesis

The aim of this study - is to investigate the impact of climate change on the solar energy potential in two locations in Sahelian part of Mali: Bamako and Mopti.

The specific objectives are:

- To evaluate the output of the 12-km spatial resolution Weather Research and Forecasting Model (WRF12km) for present day climate.
- To analyze trend and variability of temperature and solar radiation over Bamako and Mopti.
- To examine the future evolution of temperature and solar radiation over Bamako and Mopti using the RCP 4.5 scenario simulation from the 12-km spatial resolution Weather Research and Forecasting (WRF12 km) model.
- To assess the suitability of Bamako and Mopti for siting solar energy panels for both present day and future climate.

1.2.2. Research questions:

In order to appropriately investigate the impact of climate change on the potential of solar energy, the following questions were raised:

- Which are the best forcing GCMs for predicting direct (beam) and diffuse components of solar radiation and surface temperature over West Africa?
- What is the trend in surface temperature, direct (beam) and diffuse components of solar radiation over Bamako and Mopti?
- How will climate change affect solar energy potential in Bamako and Mopti?

1.2.3. Significance of Study

The use of high resolution climate simulations will greatly contribute towards understanding the variability of surface temperature, shortwave surface downward diffuse irradiance and shortwave surface downward direct irradiance and aid the assessment of solar energy potential. This information is useful in exploring the possible integration of solar energy into the national grid.

1.2.4. Scope of the study

This study will use the 12 km spatial resolution WRF output to simulate the impact of climate change on the solar energy potential over Bamako and Mopti. The physical parameters: only shortwave surface downward diffuse irradiance, shortwave surface downward direct irradiance, surface temperature were used to achieve this work. Additional parameters (including non-climatic ones) need to be taken into consideration for a holistic investigation.

1.2.5. Roadmap

The introduction has been presented in the first chapter. The second chapter is the literature review which comprise of renewable energy and solar energy development throughout the world in general and West-Africa in particular. The methodology of the study is presented in the third chapter. Results and discussions constitute the fourth chapter, while a summary of the study, conclusions and recommendations on integrating solar energy into the national grid of Mali, can be found in the last chapter.

Chapter 2

LITERATURE REVIEW

Introduction:

This chapter gives an overview of renewable energy situation in the Economic Community of West African States (ECOWAS) region, and a review of relevant literature on the subject matter.

2-1 ECOWAS RENEWABLE ENERGY:

The household sector consumes more energy of all final energy consumption for the states of Niger and Gambia. For example, the household sector in Niger account for 90 % of all final energy.
In 2012, Ghana's final energy consumption was 38.8%, transportation sector was 38.9% and industrial sector was 20%. In the other states of the ECOWAS region, the energy consumption is distributed between economic sectors and household sector in a much broader manner.

In the lead-up to developing the ECOWAS Renewable Energy Policy, the ECOWAS Centre for Renewable Energy and Energy Efficiency (ECREEE) identified several major interrelated energy challenges facing the region. The challenges included energy access, energy security on human health and the environment, and climate change. Each of these play a major role in shaping the regional energy situation and policy framework and thus, must be taken into account in any investment initiative. Sub-Saharan Africa was the only region in the world where the rate of progress in expanding access to electricity and non-solid fuels fell behind population growth between 1990 and 2010. The ECOWAS region's total final energy consumption (TFEC) reached approximately 5,687 petajoules in 2010, accounting for about 35% of the sub-Saharan total. Across the region, traditional biomass resources such as wood and charcoal play a central role in fulfilling basic energy needs. In 2010, traditional biomass accounted for more than half of TFEC in nine Member States (see Figure1). Households in particular depend heavily on these resources. In the Gambia, for example, the International Renewable Energy Agency (IRENA) estimates that traditional biomass accounts for 90% of household energy consumption (rising to 97% in some rural areas). In Cote d'Ivoire, wood and charcoal account for about 70% of household energy consumption (IRENA, 2014).

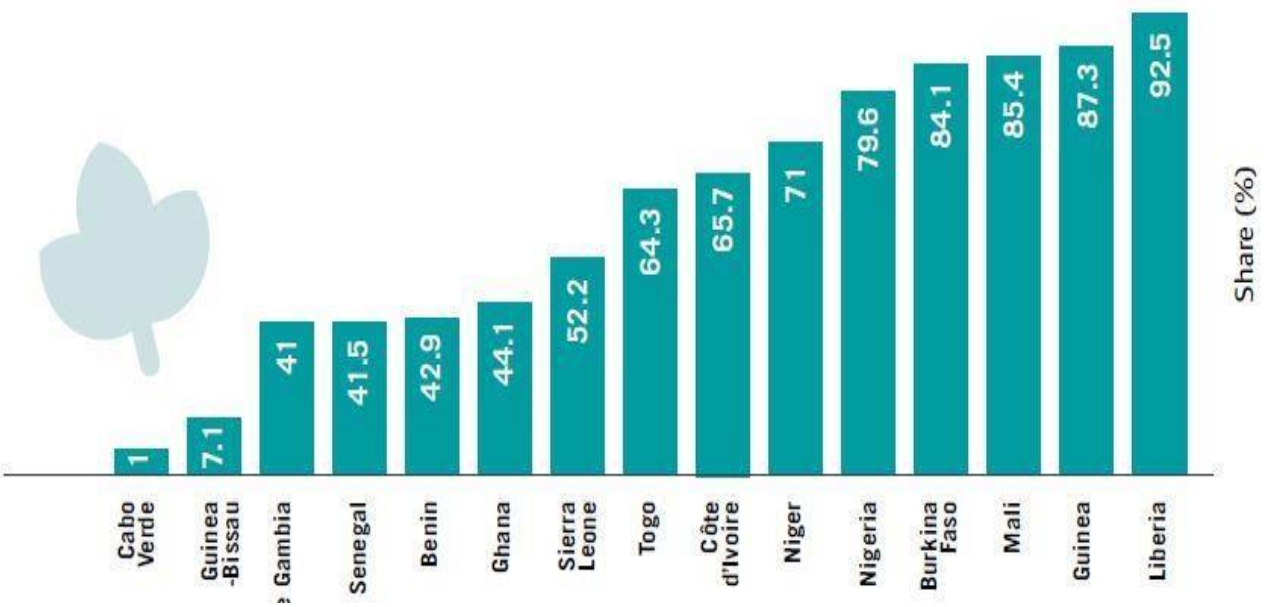

Figure 1: Share of Traditional Biomass in Total Final Energy Consumption in 2010.

Source: United Nations' Sustainable Energy for All (SE4ALL).

2.2 ENERGY SITUATION IN MALI:

The primary energy supply in Mali is biomass (figure 2) and it supplies all the energy consumed in the household sector. Electricity access rates are low but improving, electricity demand is growing extremely fast, driven by domestic consumers and the industrial and mining sectors. The national grid has a large but declining share of hydroelectricity, but both isolated centers and large capacitive generators rely exclusively on fossil fuels to satisfy their energy needs (REA, 2015).

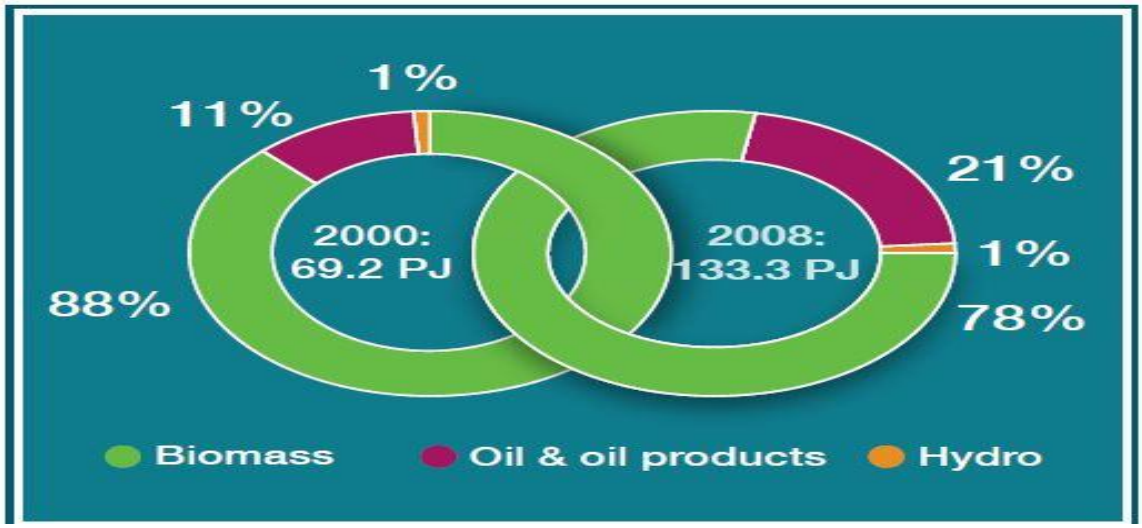

Figure 2:Total Primary Energy Supply in 2000 and 2008 (source: IRENA; 2012).

Energy Mali (EDM-SA), the organization that generates, transmits and distributes electricity in Mali, has now been privatized in an effort to improve efficiency. The electricity demand grew significantly from 785 GWh in 2008 to 1000 GWh in 2012 and the growth rate was 6.6% per year. The number of clients increased from 202000 to 290000 during the same period. The electricity demand is unexpressed and unsatisfied for both household and industrial sectors, particularly in the mining sector.

The capacity gap needed to meet demand was 111MW in 2013 which represented 45% of needs and the estimated capacity gap was 32MW in 2014 (see figure3), which represented 13.2% of needs (EDM-SA, 2013).

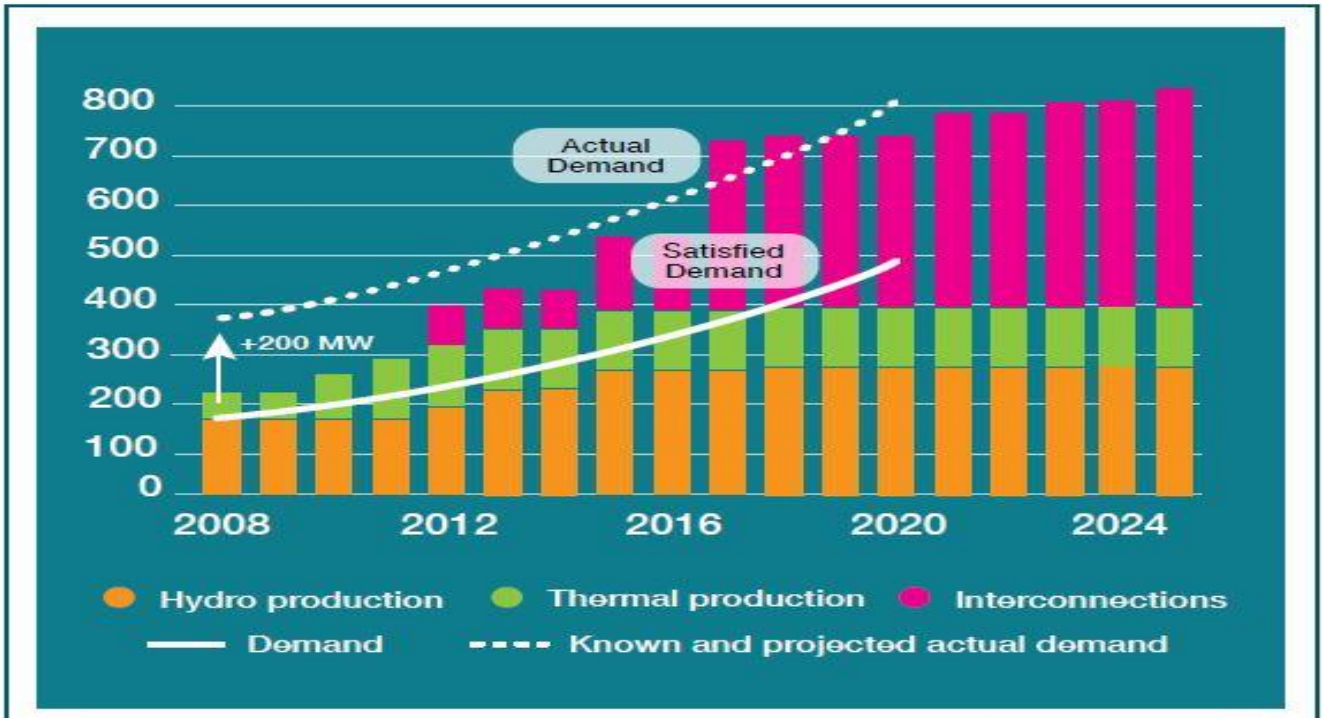

Figure 3:Energy Demand & Production Projections (MW) – On grid EDM-SA *(*Source: API, 2011*).*

2.2.1 Electricity supply:

Malian electricity sector is divided into four sub-sectors: the interconnected system, isolated centers, capacitive generation by large consumers and rural sector. EDM is the manager and the owner of the interconnected system mainly dominated by hydroelectricity generated from the Manantali (of which Mali owns 104 MW out of the total 220 MW) and Selingue (46 MW) dams. The share of hydroelectricity in the interconnected system decreased to 44% in 2014 (see Table1). This caused the Manantali Dam to encounter problems in production and important hydro plans (of Selingue and Sotuba dams), that led to delays in their 10-year maintenance schedules. To satisfy the electricity demand, EDM invested in two medium-sized thermal generation projects in 2016 for a total of 90 MW.

There are already transmission lines between Mali and its neighbors: Mauritania, Senegal and Cote d'Ivoire. To lower the cost of power in the medium term and to allow Mali to purchase more power from its neighbors, Mali planned to reinforce the connection. The mining and industrial sector use thermal generation for their energy needs (200 MW). Rural electrification uses a mix of diesel and PV (EDM-SA,2013).

Table 1:A summary of percentage contribution of different energy types to the total annual energy used (i.e. real), planned and forecasted in Mali.

	2012	2013	2014	2015	2016	2017	2018	2019	2020
	Real	Real	Plan	Forecast	Forecast	Forecast	Forecast	Forecast	Forecast
Thermal	39.8%	47.0%	55.7%	59.9%	60.6%	61.9%	50.7%	51.2%	55.2%
Hydro	60%	53.0%	44.2%	39.9%	36.3%	35.3%	46.9%	44.5%	40.9%
Solar	0%	0%	0.1%	0.2%	3.1%	2.8%	2.4%	4.3%	3.9%

GWH	1275	1402	1629	1789	1966	2197	2516	2741	2985

2.2.2 Mali Renewable Energy

A few strengths, weaknesses, opportunities and threats about Mali's renewable energy have been presented below:

(a) Strengths

- Hydro, solar and biomass have a great potential/resource
- Experience in hydro, biomass and some Photovoltaic (PV) systems
- RE available for rural access in remote areas

(b) Weaknesses

- Hydro maintenance needed.
- Unsustainable collection and use of biomass not fully addressed
- Little experience in wind power

(c) Opportunities

- Growth opportunities for all technologies
- Great interest from private sector in solar PV
- Biofuels with widespread local plants promising

(d) Threats

Climate change and extreme weather events could undermine RE potential, especially hydro and biomass.

2.3 Solar Energy Overview:

Not all solar radiation getting into the Earth's atmosphere reaches the ground. About 30% of solar radiation is reflected into space while about 20% is absorbed by clouds and molecules in the air. About three quarters of the Earth's surface is water. However, even if only 10% of total solar radiation is utilizable, 0.1% of it can power the entire world (Julian, 2011). It is interesting to compare the annual solar energy that reaches Earth with the estimated total reserve of various fossil fuels. The numbers show that the total proved reserves of fossil fuel are approximately 1.4%

of the solar energy that reaches the Earth's surface each year. Fossil fuels are solar energy stored as concentrated biomass over many millions of years. In 1983 the consumption of fossil fuel energy was approximately 300 EJ and has been increasing since then. The increase will continue until the end of 2030 (Julian, 2011). The projection from the US Department of Energy is shown in figure 4.

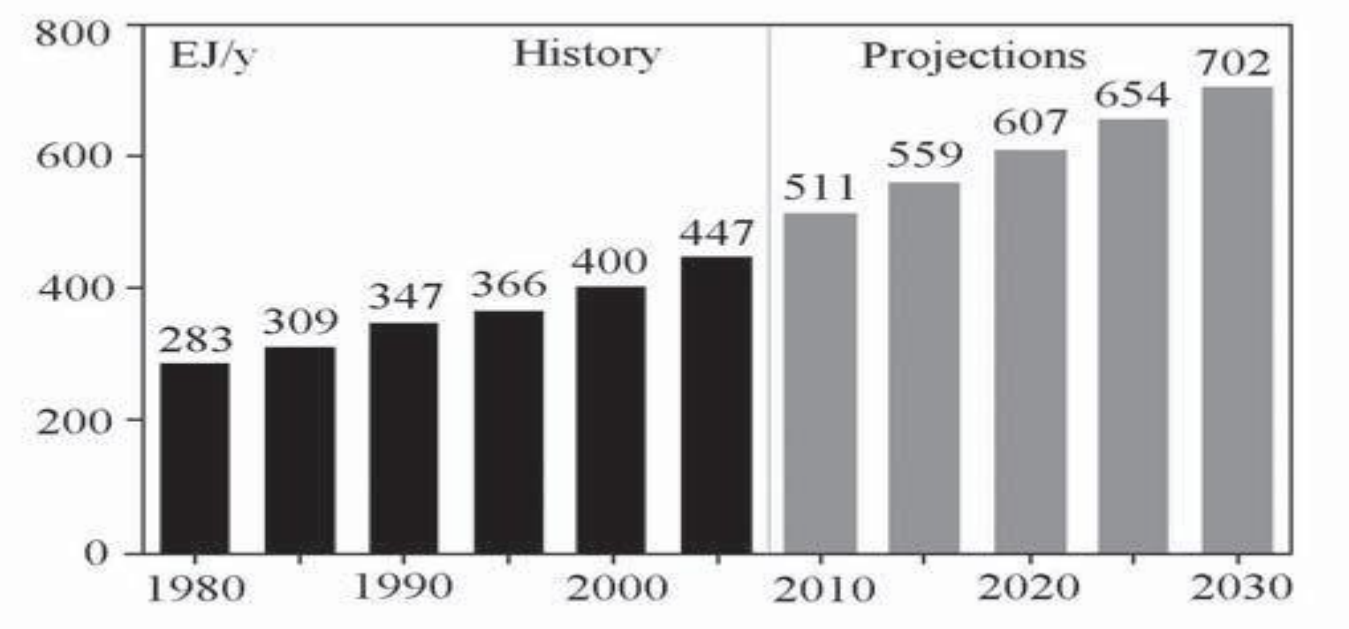

Figure 4:World marketed energy consumption from fossil fuel. Source: EIA, www.eia.doe.gov/iea.

2.3.1 Solar Energy Potential:

Technologies to convert solar energy into electricity generally fall into one of two categories: photovoltaic (PV) modules that convert light directly into electricity, and concentrating solar thermal power (CSP) systems that convert sunlight into heat energy that is later used to drive an engine. Although solar power can be generated at any scale, PV technology is modular and can be scaled for anything from household use to a large network of PV farms, whereas CSP is typically considered viable only as a utility-scale plant. Direct Normal Irradiance (DNI) values, used to measure potential for CSP, are high across the region. However, due to the scarcity of transmission

and distribution infrastructure, ECREEE estimates that CSP is currently technically feasible only within a certain geographic band in the Sahel. As of mid-2017, no Member State had developed CSP technology. The resource potential for solar PV is generally good and relatively homogenous throughout all of West Africa, except in Mali and northern Niger, where the resource is particularly strong (IRENA, 2014).

2.3.2 Installed Capacity:

Recently, several Member States have demonstrated a growing interest in grid-connected and large-scale solar projects (See Figure 5). Cabo Verde has an installed grid-connected solar PV capacity of 6.4 MW. This includes two solar farms on the islands of Santiago and Sal (4.3 MW and 2.1 MW, respectively), both developed by Portugal's Martifer Solar and commissioned in 2010. As of June 2014, Cabo Verde was planning to launch an auction for small-scale grid-connected PV projects on several islands. Ghana's Navrongo PV plant, which came on line in 2013 with an installed capacity of 1.92 MW, is the largest grid-connected solar PV installation in West Africa outside of Cabo Verde. The Volta River Authority ultimately plans to expand the plant to 2.5 MW. Several additional PV plants are scheduled to come on line in Ghana in 2017. Norwegian company Scatec Solar has an agreement in place with Ghana's Energy Commission and the country's Public Utilities Regulatory Commission (PURC) to construct a 50 MW PV plant with local partner Scatec Solar Ghana. Plans for the 155 MW Nzema solar PV park have been finalized, with construction scheduled to have begun in September 2014 with power generation expected by mid-2015. The plant is expected to have an annual generation of 240,000 megawatt-hours (MWh) (IRENA, 2014). In 2017, Burkina Faso also implemented a solar farm of 33 MW capacity (ECREEE, 2017).

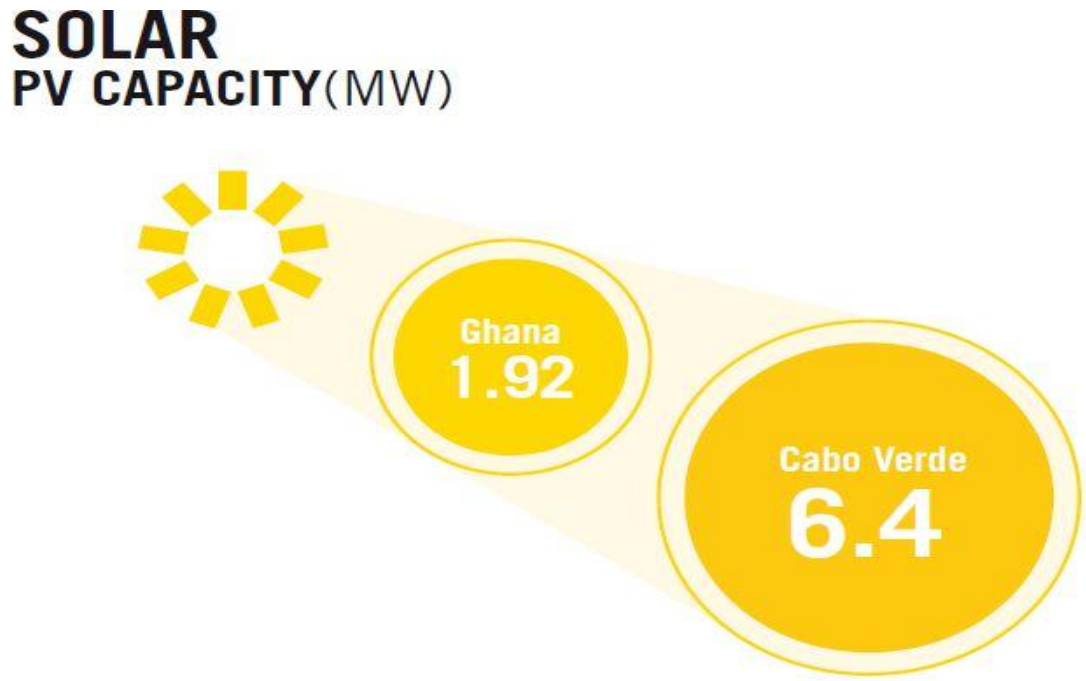

Figure 5:Installed Grid-Connected Solar PV Capacity in ECOWAS Member States, 2014 (Source IRENA,2014).

Table 2: shows the locations of the largest and smallest clean energies mini-grid (CEMG) plants in West Africa.

Table 2:Location & size of largest and smallest CEMG plants in West Africa (Eseoghene et al., 2016).

CEMG plant	Category	Country	Village	Capacity
PV-diesel	Smallest	Mali	Kandia	6.9kWp/8 kVA
	Largest	Mali	Bankass & Koro	384kWp/675 kVA each
PV only	Smallest	Nigeria	Uniarho	2.4 kWp
	Largest	Benin	Kabo	45 kWp
PV-Wind diesel hybrid	Smallest	Senegal	Sine Moussa Abdou	5 kWp/5 kW/10 kVA
	Largest	Ghana	Pediatorkope	39.5 kWp/11 kW/30 kVA
Biodiesel	Smallest	Mali	Sido	9.2 kVA
	Largest	Mali	Garalo	375 kVA

Small Hydro	Smallest	Liberia	Yandohun	60 kW
	Largest	Liberia	Firestone Plantation	4800 kW

Estimates of total installed solar PV capacity are unreliable, as few Member States collect data on self-generation or off-grid projects. However, data on distributed PV capacity in the Gambia, Guinea- Bissau, Niger, Nigeria, and Sierra Leone indicate widespread use of the technology (See Figure 6).

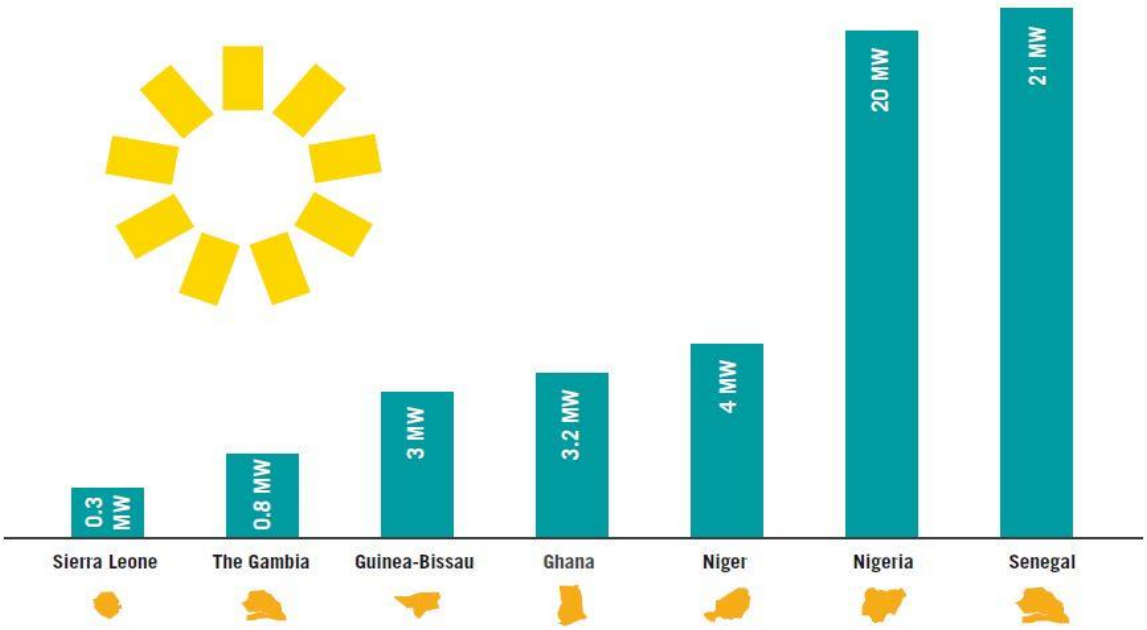

Figure 6:Estimated Installed Capacity of Distributed Solar PV in Selected ECOWAS Member States, 2012 (Sources, Gambian Ministry of Energy & Petroleum; National Focal Institution for Guinea-Bissau; IRENA; National Focal Institution for Nigeria; UNDP; ECREEE).

2.4 Climate change impacts on solar energy:

The Intergovernmental Panel on Climate Change indicates that future climate will begin to behave less like past climates in the coming decades. Modeled projections of changes in the long-term future state are attractive for national energy investments that are considering large penetration of renewable energy generation in their portfolios. Among Sub-Sahara Africa, West –Africa has been identified as one of the world most vulnerable regions to the effect of climate change (Tchotchou and Kamga, 2010). Climate change can cause the variability in weather patterns (wind speed, solar radiation, precipitation, temperature) that are the sources of RE (Lital et al., 2012). Some studies

have shown that climate change might affect the availability of RE resources in West-Africa in the future. Therefore, changes in resource potentials resulting from the impact or consequences of climate change may affect power generation from RE sources and can affect future electricity output. There is also the tendency of a change in magnitude of several weather parameters (global solar radiation, relative humidity, precipitation, and wind speeds) that contribute to building comfort in the advent of a changing climate (Ohumakin et al., 2013).

Climate conditions relevant to the productivity of solar power plants may change over the coming decades subject to anthropogenic climate change. While changes in air temperature are a widely acknowledged aspect of climate change, potential changes in surface solar radiation have been discussed to a much lesser degree. For simplicity or lack of better knowledge, surface solar radiation is often assumed to remain constant over time. However, there is growing evidence that surface solar radiation undergoes substantial multi-decadal variations, which should be considered in solar resource assessments. Coherent periods and regions with prevailing declines (known as "global dimming ") and inclines (known as "brightening ") in surface solar radiation have been detected in the worldwide observational networks, often in accordance with anthropogenic air pollution patterns. This suggests that anthropogenic air pollution and associated accumulation of aerosols in the atmosphere may have substantially contributed to the decadal variations in surface solar radiation. Specifically, the decline in surface solar radiation at widespread observation sites from the 1950s to the 1980s is in line with the strongly increasing air pollution during this period, whereas the subsequent partial recovery of surface solar resources since the 1980s fits well with the successive implementation of effective air pollution regulations, leading to decline in aerosol burdens and more transparent atmospheres particularly in industrialized countries since the 1980s (Martin et al.,2017). Solar radiation has direct impact on solar energy generation, agriculture and water resources, among others. Solar energy resources can be affected by climate change caused by enhanced CO_2 concentration in the atmosphere. The impact of climate change at seasonal time scales can impact the socio-economic sectors. Thus, changes in solar radiation in future climate is important and of considerable interest (Pan et al., 2004). Clouds cover about 60% of the earth's surface (Rossow and Schiffer,1999; Vardavas and Taylor,2011) and can strongly affect the radiation budget of the earth atmosphere system. The earth's climate is sensitive to cloud distributions and cloud radiative properties associated with anthropogenic forcing arising from changes in greenhouse gases and aerosols. They are highly variable and small changes in the

properties can significantly affect climate (Pyrina et al.,2013). Global diffuse and direct irradiance are correlated with cloud cover and sunshine duration. (e.g. Löf et al., 1966). Changes in the amount of cloud cover can cause trends in solar radiation (Stanhill and Cohen, 2001).

To estimate potential future changes in surface solar radiation and related meteorological quantities relevant for solar power production, however, we can obviously no longer use past observations alone, but have to rely on projections from comprehensive climate models. These models have become the primary tools for the development of climate change scenarios for the 21st century, such as those for the latest IPCC assessment five report (AR5), with the latest model generation known as the Coupled Model Inter-comparison Project Phase 5 CMIP5 models (Wild et al., 2015).

In order to predict the future solar irradiance fields needed for long range planning of solar energy use; there is need for the quantification of the potential changes of solar radiation in the enhanced CO_2 atmosphere (Ohumakin et al.,2015). The quantification requires the use of climate models. This is because climate model output constitutes consistent datasets of atmospheric variables coupled with the few in situ observation stations and most times, poor quality of available data. Climate models (global and regional circulation models) can help to understand processes that govern the climate systems (Pal et al.,2007). Several number of simulations have been carried out using Global circulation models (GCMs). However, (GCMs) have difficulties to reproduce various atmospheric variables of interest at a reasonable spatial resolution and thus cannot generate realistic outputs (Olayinka et al.,2015).

Seldom et al, (2011) linked 10 GCM-scenario pairs to an RCM to estimate climate change effects on the Norwegian energy sector. Changes in wind, solar irradiation, and heating and cooling demand, among others, were estimated by interpolating the RCM results to twenty (20) geographic locations: Seven (7) for solar, and thirteen (13) for wind. The study found that while Global Horizontal Irradiance (GHI) and hydropower changes were significant in some of the GCM-scenario projections, changes in wind were minor, with the maximum change for all locations and months around 4.8% by 2050. Pan et al, (2004) used a refined regional climate model to estimate

seasonal changes in GHI simply by raising greenhouse gas concentrations in the regional model. A decreasing trend was found in the seasonal-mean of GHI of about 0–20% over the entire United States. This trend was most noticeable in the western U.S. during fall, winter, and spring. There have been few studies that have looked at future changes in solar resource, likely due to the uncertainties in GCM cloud cover estimations. (Charles et al., 2015).

Ioanna et al, (2014) examined the effect of projected changes in irradiance and temperature on the performance of photovoltaic systems in Greece. Climate projections were obtained from 5 regional climate models (RCMs) under the A1B emissions scenario, for two future periods. The RCM data presented systematic errors against observed values, resulting in the need for bias adjustment. The projected change in photovoltaic energy output was then estimated, considering changes in temperature and insolation. The spatiotemporal analysis indicated significant increase in mean annual temperature (up to 3.5∘C) and mean total radiation (up to 5W/m2) by 2100. The performance of photovoltaic systems exhibits a negative linear dependence on the projected temperature increase which is outweighed by the expected increase of total radiation resulting in an up to 4% increase in energy output; Martín, et al., (2016) evaluated WRF model for forecasting solar radiation in the Iberian Peninsula. They did an evaluation of ERA-40 reanalysis data from European Center for Medium Range Weather Forecasting ECMWF and WRF mesoscale model over 40 stations from Spanish National Radio Metrical Network which belongs to the Spanish National Weather Service (AEM). The evaluation was done at hourly and daily temporal resolution for the WRF and ERA-40 data respectively. The results from WRF model were compared with predictions from ECMWF. WRF model had been validated for a whole year over Spain; Ruiz-Arias, et al., (2012) assessed the Improvement of the WRF model for solar resource assessments and forecasts under clear sky. Their aim was to improve the shortwave downward solar radiation assessment and forecasting by equipping the model with a mechanism to ingest both high temporal and high spatial resolution aerosol data. This resulted in a reduction of the bias caused by any misrepresentation of the aerosol optical properties and their spatio-temporal variability. The main impact of this improvement is on the direct and diffuse components of solar radiation. They presented a preliminary study over the Continental United States using the Goddard Space Flight Center shortwave scheme, MODIS Level 3 aerosol optical depth data, and three ground stations of NOAA's SURFRAD radiation network. Results under cloudless conditions showed a relative

improvement in the mean bias error of about 80% in the direct normal irradiance and up to about 70% in the diffuse irradiance; Zempila, et al., (2016) evaluated WRF shortwave radiation parameterizations in the prediction of Global Horizontal Irradiance in Greece. They assessed the differences induced in the Global Horizontal Irradiance (GHI) predictions by the mesoscale atmospheric Weather Research and Forecasting (WRF) model while using different shortwave radiation. Model predictions were compared with GHI measurements at 12 stations of the Hellenic Network of Solar Energy (HNSE) for January, April, July and October 2013. The shortwave radiation schemes that were evaluated are: The Dudhia, the updated Rapid Radiative Transfer Model (RRTMG), the updated Goddard and the Goddard Fluid Dynamics Laboratory (GFDL) schemes. All schemes performed well under cloudless conditions this was due to limited ability of the WRF model to simulate cloudy conditions. The Dudhia scheme performed best with mean relative difference of 2.2 ± 15% for clear skies, while the differences for the other schemes range between 5 and 12% with similar standard deviations. For all- cloudy skies), the model-derived hourly GHI is overestimated for all schemes (40-70%).

Chapter 3

METHODOLOGY

3.1 Study Area:

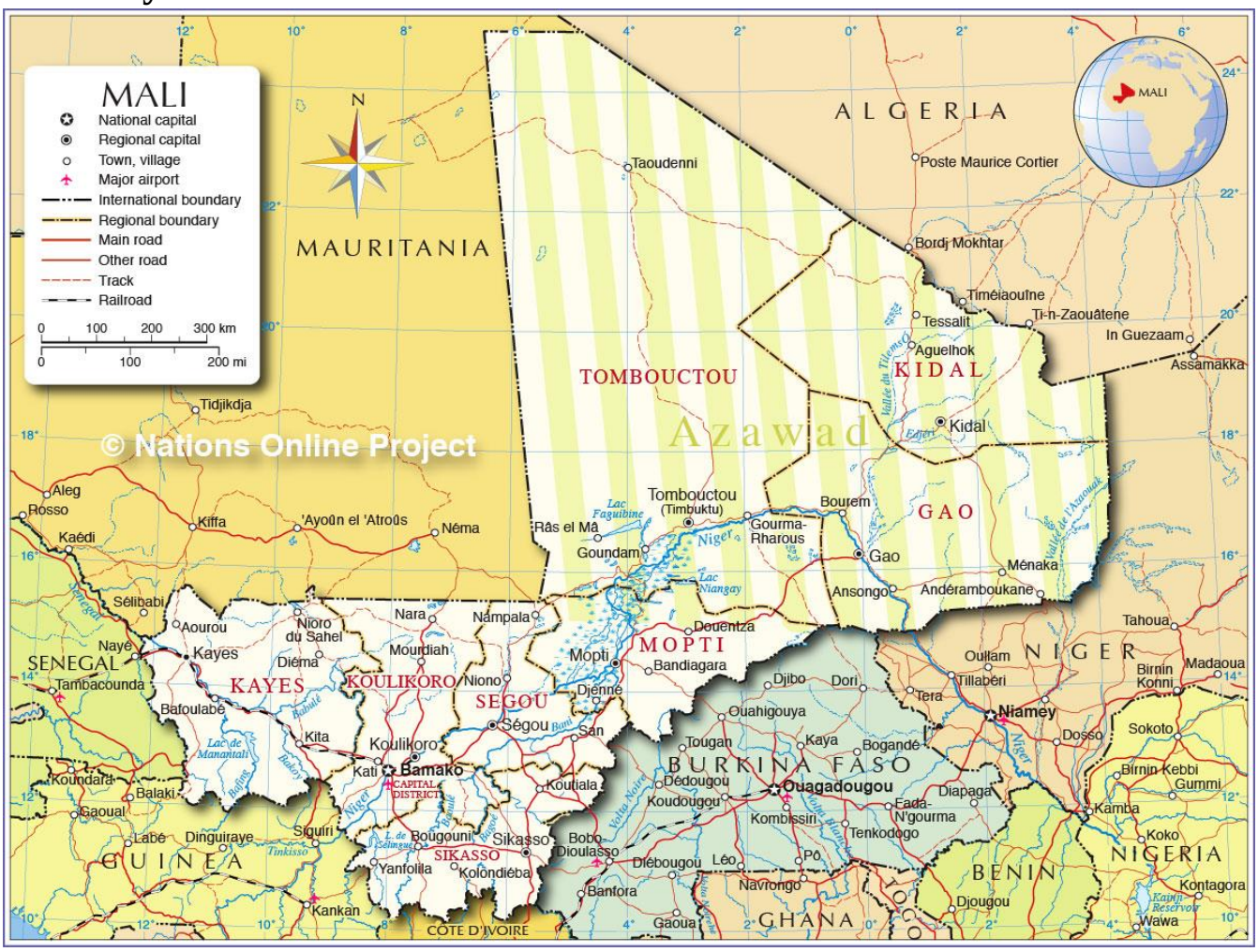

Figure 7:Map of MALI *(http://www.nationsonline.org/oneworld/map/mali_map.htm).*

Mali is a landlocked country in the Sahel region of West Africa. It covers an area of 1,241,248 km^2, 51% of which is desert. Its population is estimated at 14.5 million and its average annual growth rate is 3.4%. Mali's economy is mainly based on agriculture and fishing. Mali's climate is characterized by a long dry season and a rainy season that lasts on average one to five months per

year, depending on the region. On the basis of rainfall amount, the country is divided into four main areas corresponding to four ecological zones (zone Saharienne, zone Sahelian, zone Soudanienne and zone Soudano-Guineenne) with diverse agricultural potential.

The energy sector of the country comprises four main sub-sectors, the four sub-sectors are Fossil fuel, traditional energy, renewable energy and Electricity.

- **Fossil fuel:** The oil and gas sub-sector is characterized by total dependence on petroleum imports.
- **Traditional energy:**

Fuel wood is the primary traditional energy source for households. Mali's forestry potential is estimated at roughly 33,000,000 hectares (ha), including a standing volume of about 520,000,000 m^3. The wood fuel (firewood and charcoal) is vulnerable to climatic variability.

- **Renewable energy:** The national renewable energy inventory reveals substantial potential depending on the source of energy.

Although these sources have never been factored into the energy mix, they may be about 3% of conventional electricity generation or 12 megawatts (MW).

- **Electricity:**

The national electricity access rate was 27.1% in 2010. The demand for electricity is growing by 10% annually. The electricity access rate is around 55% in urban areas, but only 14% in rural areas. It is worth noting that hydroelectricity is vulnerable to climatic variability.

3.2 Solar Energy:

According to well-established measurements, the average power density of solar radiation just outside the atmosphere of the Earth is 1366 W/m^2, widely known as the *solar constant*. The definition of the meter is one over 10,000,000 of Earth's meridian, from the North Pole to the equator, see Fig. 8. This definition is still pretty accurate according to modern measurements.

Therefore, the radius of the Earth is $(2/\pi) \times 10^7$ m. The total power of solar radiation reaching Earth is then:

$$\text{Solar power} = 1366\times\frac{4}{\pi}\times 10^{14} \cong 1.73\times 10^{17}\text{W} \quad (3.1)$$

Each day has 86,400 s, and on average, each year has 365.2422 days. The total energy of solar radiation reaching Earth per year is:

$$\text{Annual solar energy} = 1.7310^{17}\times 86400\times 365.2422 \cong 5.4610^{24}\text{J} \quad (3.2)$$

Or 5,460,000 EJ/year. To have an idea of how much energy that is, let us compare it with annual global energy consumption. In the years 2005–2010, the annual energy consumption of the entire world was about 500 EJ. A mere 0.01% of the annual solar energy reaching Earth can satisfy the energy need of the entire world the average solar power on the Earth is 1366 W/m2 (see figure 8). The length of the meridian of Earth, according to the definition of the meter, is 10,000,000 m. The total solar energy that arrives at the surface of Earth per year is 5,460,000 EJ (Julian, 2011).

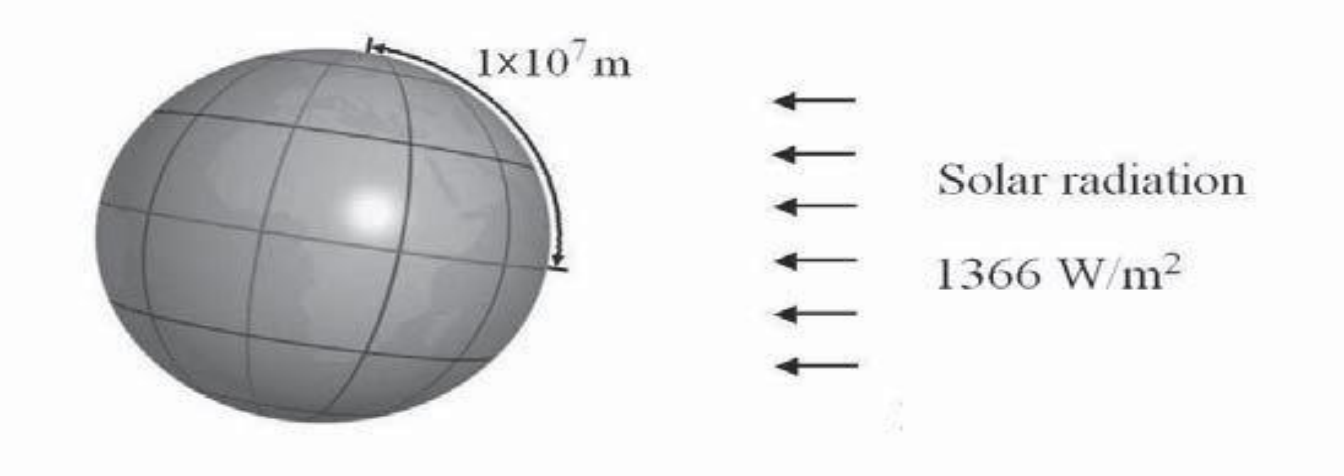

Figure 8:Annual solar energy arriving at surface of Earth.

3.3 Data and Model Description:

3.3.1 ECMWF Reanalysis Data (ERA-Interim)

ERA 40 is a second-generation reanalysis. It is the first reanalysis to directly assimilate satellite radiance data (TOVS, SSM/I, ERS and ATOVS). Cloud Motion Winds were also used. The result is better circulation over the tropics and southern hemisphere. However, unless comparing to previous ERA-40 based results, it is recommended that the 3rd generation reanalysis, ERA-Interim or MERRA, be used for new research. In this study, the MERRA data was used.

3.3.2 Global Climate Models:

Table 3:Global Climate Models Used (Bazyomo et al., 2016).

Modelling Centre	Institution	Model
NOAA GFDL	Geophysical Fluid Dynamics Laboratory	GFDL-ESM2M
MOHC (additional Realizations by INPE)	Met Office Hadley Centre (additional HadGEM2-ES realizations contributed By Instituto Nacional de Pesquisas Espaciais)	HadGEM2-ES
MPI-M	Max Planck Institute for Meteorology (MPI-M)	MPI-ESM MR

3.3.3 Regional Climate Model-WRF:

The version 3 of the Advanced Research WRF (ARW) modeling system has been available since April 2008. The ARW is designed to be a flexible, state-of-the-art atmospheric simulation system that is portable and efficient on available parallel computing platforms. The ARW is suitable for use in a broad range of applications across scales ranging from meters to thousands of kilometers, including: Idealized simulations (e.g. LES, convection, baroclinic waves), Parameterization research, Data assimilation research, forecast research, Real-time NWP, Hurricane research, Regional climate research, Coupled-model applications, Teaching

The Mesoscale and Microscale Meteorology Division of NCAR is currently maintaining

and supporting a subset of the overall WRF code (Version 3) that includes: WRF Software Framework (WSF); Advanced Research WRF (ARW) dynamic solver, including one-way, two-way nesting and moving nest; The WRF Preprocessing System (WPS); WRF Data Assimilation (WRF-DA) system which currently supports 3DVAR, 4DVAR, and hybrid data assimilation capabilities; Numerous physics packages contributed by WRF partners and the research

Community; Several graphics programs and conversion programs for other graphics tools.

The WRF modeling system software is in the public domain and is freely available for community use.

The following figure 9 below shows the flowchart for the WRF Modeling System Version 3.

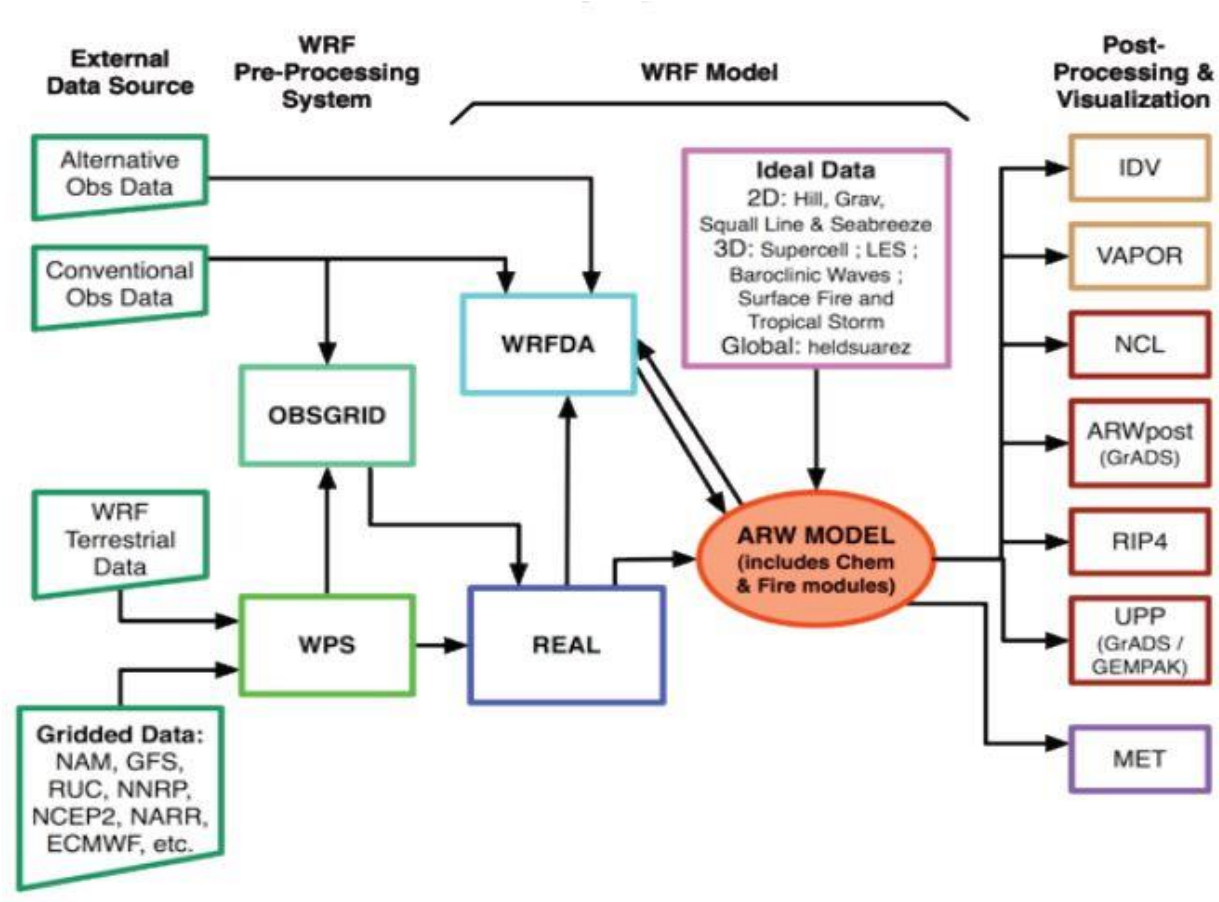

Figure 9:The flowchart for the WRF Modeling System Version 3.

3.4 Experiments:

3.4.1 Ensemble experiment design:

The WASCAL ensemble presented here consists of a combination of three GCMs (MPI, GFDL, HAD-GEM) with one RCM (WRF). The climate change scenario RCP4.5 (Representative Concentration Pathway 4.5; van Vuuren et al., 2011) was used. The choice of RCP4.5 was made because of limited computational resources and is based on the fact that:

- the differences between RCP4.5 and RCP8.5 become apparent only after 2040, and

- that the RCP4.5 scenarios – in light of the COP21 agreement made in Paris in December 2015 – is a reasonable scenario.

The selected GCMs, on the other hand, cover the extremes in temperature and precipitation of the GCM ensemble used in CORDEX and span a larger range of conditions until about 2060 than the two scenarios (i.e. RCP 4.5 and RCP 8.5) and are able to reproduce the dominant, large-scale atmospheric features over West Africa (Nikulin et al., 2013; Elguindi et al., 2014). Furthermore, a control run using re-analysis data is included for model verification and future bias correction.

The control run using re-analysis forcing data is conducted for the period 1979-2014. The historical runs are generated for the period 1979-2005 and extended by the RCP4.5 runs until 2010. This approach allowed to derive statistics for the climatological reference period 1980–2010 (, as defined by the World Meteorological Organization (2011). Future projections are calculated for the periods 2019–2050 and 2069–2100 to provide similar 30-year windows for the mid and end of the 21st century. It should be noted that the three selected GCMs are based on different calendars, which makes model verification and comparison difficult on timescales shorter than one month: While the MPI-ESM MR model (as well as ERA-Interim) employs a Gregorian calendar, the GFDL-ESM2M and HadGEM2-ES models are based on a 365-day (no-leap year) and a 360-day (12×30 days) calendar, respectively.

The generation of an ensemble of climate projections at a resolution of 12 km and for at least 90 years in total is a process over several years and requires the use of different high-performance computing (HPC) centers. To ensure consistency within each model run, the entire integration for a particular combination of GCM and RCM is conducted on the same system (Heinzeller et al., 2017).

3.4.2 WRF model configuration:

In limited area modelling, the size of the computational domain can have a significant influence on the quality of the results (Leduc and Laprise, 2008). In a recent study, Browne and Sylla (2012) demonstrated that the ability of a RCM to spin up the regional- and large-scale patterns associated with the West African Monsoon flow depend on a suitably large extent of the RCM domain. Figure 10 displays the nested domain configuration for the ensemble experiment, using an outer domain at 60 km resolution to downscale the coarse global forcing data sets and to provide boundary and initial conditions for the inner domain at 12 km horizontal resolution. The figure also highlights

the three dominant agro-climatological regions in West Africa, following a north-south gradient in annual precipitation. In addition to the domain configuration, a common standard for the model output was defined for all model runs to facilitate the use of the results. All data is provided in a netCDF CF-1.6 compliant format on a regular latitude-longitude grid for a pre-defined, extensive set of variables and pressure levels.

An inherent problem of limited area modelling is that supplying lateral boundary conditions to nested models can cause severe problems, up to the point where the RCM solution becomes inconsistent with the forcing data. This is problematic for long-term transient simulations associated with a large computational domain (Davies, 1983; Warner et al., 1997; Harris and Durran, 2010; Park et al., 2014). The different approaches to address this issue that are discussed in the literature, range from daily to weekly re-initialisation, sometimes even including soil conditions (Otte, 2008), to transient runs covering the entire period of interest (Giorgi et al., 2009; Dieng et al., 2017). In general, more frequent re-initialisation is suitable for studying individual weather events, whereas a longer re-initialisation is useful in climate applications. Here, we adopt an intermediate solution by conducting 11-year time slice experiments, which allows for one year spin up of the soil conditions each time.

For instance, the ERA-Interim-driven control run, providing data for the period 1980–2014, consists of the four-time slice experiments 1979–1990 (S1), 1989–2000 (S2), 1999-2010 (S3), 2009–2014 (S4). In this work we averaged the 1990 from S1 and the 1990 from S2. Together with a spectral nudging approach on the outer domain (Miguez-Macho et al., 2004; von Storch et al., 2000; Otte et al., 2012), this approach allows the WRF model to spin up and evolve the necessary fine-scale structures, embedded in the large-scale features of the forcing global model, without departing too far from the global conditions. An optimal configuration of the WRF model is paramount to address key questions regarding the impact of climate change.

For the West African region, one of the important things is an accurate representation of the West African Monsoon (WAM) features in the model. In several studies it was shown that the choice of physical parameterizations available in WRF can greatly influence the model's skills, mostly measured in near-surface temperature and precipitation accuracy (Noble et al., 2014; Klein et al., 2015). This setup is based on the Klein et al. (2015) WRF parameter study of 27 combinations of microphysics, planetary boundary layer and cumulus schemes for two extreme years (dry and wet),

forced by ERA-Interim re-analysis data. To account for the different characteristics and resolutions of re-analysis data and GCM data, we extended their study and tested their most promising configurations using MPI-ESM MR (close to the CMIP5 multi model mean; Nikulin et al., 2013) as forcing data. The resulting optimal setup of WRF used in the WASCAL high-resolution ensemble experiment is thus a compromise to obtain good performance for both ERA-Interim and MPI-ESM MR forcing, and also accounts for the higher resolution (12 km versus 24 km in Klein et al., 2015).

WRFV3.5.1 supports Gregorian and 365-day calendar types, but not the 360-day calendar type employed by the HadGEM2- ES model. It was therefore necessary to add an implementation of the 360-day calendar to WRFV3.5.1. The 360-day calendar caused further complication to the pre-processing of the GCM data, since the grib standard does not support this calendar type.

The forcing model data was obtained from different sources and in different formats. ERA-Interim re-analysis data was downloaded from the European Centre for Medium-Range Weather Forecast ECMWF MARS archive2, while MPI-ESM MR data was obtained from DKRZ's CERA archive3, both in grib format. GFDL-ESM2M and HadGEM2-ES data were downloaded from the Earth System Grid Foundation (ESGF) 4 in netCDF format. This implied slightly different pre-processing steps for using the data as boundary conditions in WRF. For ERA-Interim and MPI-ESM MR, the standard pre-processing chain of WRF could be used, which consists of converting forcing model grib data to an intermediate format ("un-grib") used by the WRF preprocessing system WPS, which in turn is interpolated horizontally and vertically. For GFDL-ESM2M and HadGEM2-ES data, a separate tool was implemented to convert the netCDF data directly into the WPS intermediate format ("un-netcdf"), thereby avoiding the problem of an unsupported 360-day calendar in the grib standard.

To generate model output in a standard format, latest developments in the WRF model were employed and extended further:

WRFV3.5.1 provides the capability to interpolate model-level data to pressure levels during the integration. This capability was extended to include additional variables (in particular hydrometeors). Further, climate diagnostics such as minimum and maximum daily temperatures are calculated using the climate diagnostics features of the model. While these interpolations require additional calculations during the integration that slow down the model integration, it was

found that writing smaller amounts of data to disk (25 pressure levels instead of 40 model levels) overcompensated this increase and led to a faster model integration. The WRF model output was further post-processed by a suite of parallelised Python utilities to calculate additional variables, add CMIP5/CORDEX variable attributes and provide the desired netCDF-CF compliance (Heinzeller et al.,2017).

Table 4: List of output variables of the WASCAL WRF climate simulations. The variable types are “acc” (accumulated values), “coord” (coordinate variables), “const” (constant values), “min” (minimum over last output interval), “max” (maximum over last output interval) (Heinzeller et al.,2017).

WRF name	Output name	Units	Stream	Type	Description (long name)
ACLWDNB	rlds	J m-2	wrfsfc	acc	Accumulated surface downwelling longwave radiation
ACLWDNT	rldt	J m-2	wrfsfc	acc	Accumulated TOA incident longwave radiation
ACLWUPB	rlus	J m-2	wrfsfc	acc	Accumulated surface upwelling longwave radiation
ACLWUPT	rlut	J m-2	wrfsfc	acc	Accumulated TOA outgoing longwave radiation
ACSWDNB	rsds	J m-2	wrfsfc	acc	Accumulated surface downwelling shortwave radiation
ACSWDNT	rsdt	J m-2	wrfsfc	acc	Accumulated TOA incident shortwave radiation
ACSWUPB	rsus	J m-2	wrfsfc	acc	Accumulated surface upwelling shortwave radiation
ACSWUPT	rsut	J m-2	wrfsfc	acc	Accumulated TOA outgoing shortwave radiation
ALBEDO	alb	1	wrfsfc	inst	Albedo
CANWAT	canwat	kg m-2	wrfsfc	inst	Canopy water
CLDFRA	cl	1	wrfprs	inst	Cloud area fraction
DEPTH	depth	m	wrfsfc	coord	Depth
EMISS	ems	1	wrfsfc	inst	Surface emissivity
GHT	zg	m	wrfprs	inst	Geopotential height
GRDFLX	hfg	W m-2	wrfsfc	inst	Ground heat flux
HFX	hfss	W m-2	wrfsfc	inst	Surface upward sensible heat flux
HGT	orog	m	wrfsta	inst	Terrain height
ISLTYP	sltype	1	wrfsta	const	Dominant soil category
IVGTYP	vegtype	1	wrfsta	const	Dominant vegetation category
LANDMASK	sftlf	1	wrfsta	const	Land binary mask (1 for land, 0 for water)
LAT	lat	degrees_north	wrfclm, wrfprs, wrfsfc, wrfsta	coord	Latitude, south is negative
LH	hfls	W m-2	wrfsfc	inst	Surface upward latent heat flux
LON	lon	degrees_east	wrfclm, wrfprs, wrfsfc, wrfsta	coord	Longitude, west is negative
MU	amdry	Pa	wrfsfc	inst	Dry air mass in column
PBLH	zmla	m	wrfsfc	inst	Atmosphere boundary layer thickness
PLEV	plev	hPa	wrfprs	coord	Pressure

PMSL	psl	Pa	wrfsfc	inst	Sea level pressure
PSFC	ps	Pa	wrfsfc	inst	Surface air pressure
Q2	vaps	kg kg-1	wrfsfc	inst	Near-surface water vapor mixing ratio
QCLOUD	clw	kg kg-1	wrfprs	inst	Cloud water mixing ratio
QFX	mfs	kg m-2 s-1	wrfsfc	inst	Surface upward moisture flux
QICE	cli	kg kg-1	wrfprs	inst	Ice mixing ratio
QRAIN	clr	kg kg-1	wrfprs	inst	Rain water mixing ratio
QSNOW	cls	kg kg-1	wrfprs	inst	Snow mixing ratio
QVAPOR	vap	kg kg-1	wrfprs	inst	Water vapor mixing ratio
RAIN	pr	mm	wrfsfc	acc	Accumulated precipitation
RH	hur	%	wrfprs	inst	Relative humidity
RH2	hurs	%	wrfsfc	inst	Near-surface relative humidity
SEAICE	sic	1	wrfsfc	inst	Sea ice binary mask (1 for sea ice, 0 for water)
SHDMAX	vegmax	1	wrfsta	const	Annual max vegetation fraction
SHDMIN	vegmin	1	wrfsta	const	Annual min vegetation fraction
SKINTEMPMAX	tsmax	K	wrfclm	max	Daily maximum surface skin temperature
SKINTEMPMIN	tsmin	K	wrfclm	min	Daily minimum surface skin temperature
SMCREL	mrrlsl	1	wrfsfc	inst	Relative soil moisture
SMOIS	mrlsl	m3 m-3	wrfsfc	inst	Water content of soil layer
SMOIST	mrso	m3 m-3	wrfsfc	inst	Total soil moisture content
SNOALB	albmax	1	wrfsta	const	Annual max snow albedo in fraction
SNOW	snw	kg m-2	wrfsfc	inst	Snow water equivalent
SNOWH	snd	m	wrfsfc	inst	Physical snow depth
SPDUV	wind	m s-1	wrfprs	inst	Wind speed
SPDUV10	sfcWind	m s-1	wrfsfc	inst	Near-surface wind speed
SPDUV10MAX	sfcWindmax	m s-1	wrfclm	max	Daily maxmimum near-surface wind speed
SR	prfz	1	wrfsfc	inst	Fraction of frozen precipitation
SST	tso	K	wrfsfc	inst	Sea surface temperature
SWDDIF	swddif	W m-2	wrfsfc	inst	Shortwave surface downward diffuse irradiance
SWDDIR	swddir	W m-2	wrfsfc	inst	Shortwave surface downward direct irradiance
SWDDNI	swddni	W m-2	wrfsfc	inst	Shortwave surface downward direct normal irradiance
T	ta	K	wrfprs	inst	Air temperature
T2	tas	K	wrfsfc	inst	Near-surface air temperature
T2MAX	tasmax	K	wrfclm	max	Daily maximum near-surface air temperature
T2MIN	tasmin	K	wrfclm	min	Daily minimum near-surface air temperature

TCLDFRA	clt	1	wrfsfc	inst	Total cloud fraction
TD	td	K	wrfprs	inst	Dew point temperature
TD2	tds	K	wrfsfc	inst	Near-surface dew point temperature
TH2	thetas	K	wrfsfc	inst	Near-surface potential temperature
TIME	time	hours since 1970-01-01	wrfclm, wrfprs, wrfsfc, wrfsta	inst	Time
TMN	tsll	K	wrfsfc	inst	Temperature of soil at lower boundary
TSK	ts	K	wrfsfc	inst	Surface skin temperature
TSLB	tsl	K	wrfsfc	inst	Temperature of soil
U	ua	m s-1	wrfprs	inst	Eastward wind
U10	uas	m s-1	wrfsfc	inst	Eastward near-surface wind
U10MAX	uasmax	m s-1	wrfclm	max	Daily maximum eastward near-surface wind
V	va	m s-1	wrfprs	inst	Northward wind
V10	vas	m s-1	wrfsfc	inst	Northward near-surface wind
V10MAX	vasmax	m s-1	wrfclm	max	Daily maximum northward near-surface wind
VEGFRA	veg	1	wrfsfc	inst	Vegetation fraction
W	wa	m s-1	wrfprs	inst	Upward wind

3.4.3 Description of nesting strategy and time-slices:

. The high-resolution, D2 runs (12 km) were carried out as a nested simulation, using the output of the coarser resolution, D1(60 km) model runs as forcing data set. The coarser resolution model runs are forced by the different re-analysis and GCM data sets described above. An offline-nesting approach is adopted, which implies no feedback from the 12 km experiments to the 60 km

experiments. Thus, the 60 km experiments can be considered as standalone experiments at a relatively coarse resolution.

The experiments are conducted as time-sliced runs of 11-year duration each, where the first year is considered as spin up period and should not be used in the analysis. The historical run 1999-2006 is carried over into the projection run 2006– 2010 to be able to provide model data for the WMO reference period 1980–2010 by combining the three-decadal time-slice experiments 1979–1990, 1989–2000, 1999–2010 the average from the 1979-1990 to 1989-2000 were used in this work and neglecting the spin up year for each of them (Heinzeller et al.,2017).

Table 5: Description of streams into which the WASCAL WRF output variables are classified (Heinzeller et al.,2017).

Stream name	Description	Output interval
wrfclm	climate variables (extremes), two-dim.	day
wrfprs	pressure level variables, three-dim.	6hr
wrfsfc	surface, subsurface and other two-dim. variables	3hr
wrfsta	static variables, two-dim.	fx

Table 6: Description of time-slices generated in the WASCAL WRF ensemble experiment, including spinup period (HeinzEller et al.,2017).

Scenario	Time-slices
Control (ctrl)	1979–1990, 1989–2000, 1999–2010, 2009–2014
Historical (hist)	1979–1990, 1989–2000, 1999–2005 (continued by 2006–2010)
Projection (rcp4.5)	2006–2010 (continued from 1999–2005), 2019–2030, 2029–2040, 2039–2050, 2069–2080, 2079–2090, 2089–2100

Table 7: Re-analyses and global circulation models (earth system models) used as forcing data for the long-term regional climate simulations, and regional climate model used to conduct the

ensemble experiment. The characteristics of the forcing models for Africa and their climate change signal (CCS) are taken from Elguindi et al. (2014); OBS denotes observations, MMM the CMIP5 multi-model ensemble mean (Heinzeller et al,2017).

GCM/ESM	Characteristics for West Africa	CCS	Reference
ERA-Interim	re-analysis, "perfect atmosphere"	—	Dee et al. (2011)
MPI-ESM MR	temp. close to OBS/MMM	medium	Stevens et al. (2013)
HadGEM2-ES	precip. close to OBS/MMM	large	Jones et al. (2011)
GFDL-ESM2M	both differ from OBS/MMM	small	Anon (2012)
RCM	**Model configuration for West Africa**		**Reference**
WRFV3.5.1	see Table 9		Skamarock et al. (2008)

Table 8: Computational resources used for the WASCAL high-resolution regional climate ensemble experiment. Control runs are conducted for the period 1979–2014, historical runs for the period 1979–2010 (for details, see section 3), and RCP4.5 projection runs for the period 1979–2010 (for details, see section 3), and RCP4.5 projection runs for the periods 2019–2050 and 2069–2100.

GCM/ESM	RCM	Experiment	HPC
ERA-Interim	WRFV3.5.1	control	DKRZ Blizzard
MPI-ESM MR	WRFV3.5.1	hist./proj.	JSC Juropa
GFDL-ESM2M	WRFV3.5.1	hist./proj.	JSC Juropa
HadGEM2-ES	WRFV3.5.1	hist./proj.	JSC Jureca
Preprocessing			KIT/IMK-IFU Kea
Postprocessing			DKRZ Mistral

DKRZ: German Climate Computing Centre, http://www.dkrz.de; JSC: Jülich Supercomputing Centre of the Research Centre Jülich, http://www.fz-juelich.de/ias/jsc; SCC: Steinbruch Centre for Computing of the Karlsruhe Institute of Technology, http://scc.kit.edu.

Table 9: WRF model configuration for the two domains at 60 km and 12 km resolution (Heinzeller et al, 2017).

Run	wrf-60km	wrf-12km
Microphysics	WSM5	WSM5
Radiation	RRTMG LW/SW	RRTMG LW/SW
Cumulus	Grell-Devenyi	Grell-Devenyi
PBL	ACM2 (Pleim)	ACM2 (Pleim)
Surface layer	Janjic Eta	Janjic Eta
Land-surface	Noah LSM	Noah LSM
Grid FDDA	UV/T/PH above PBL	off
o3input	2	2
aer_opt	1	1
Domain size	$157 \times 106 \times 40$	$496 \times 331 \times 40$
Time step	360 s	72 s
Rad. time step	24 m	24 m
LBC* interval	6 h	3 h

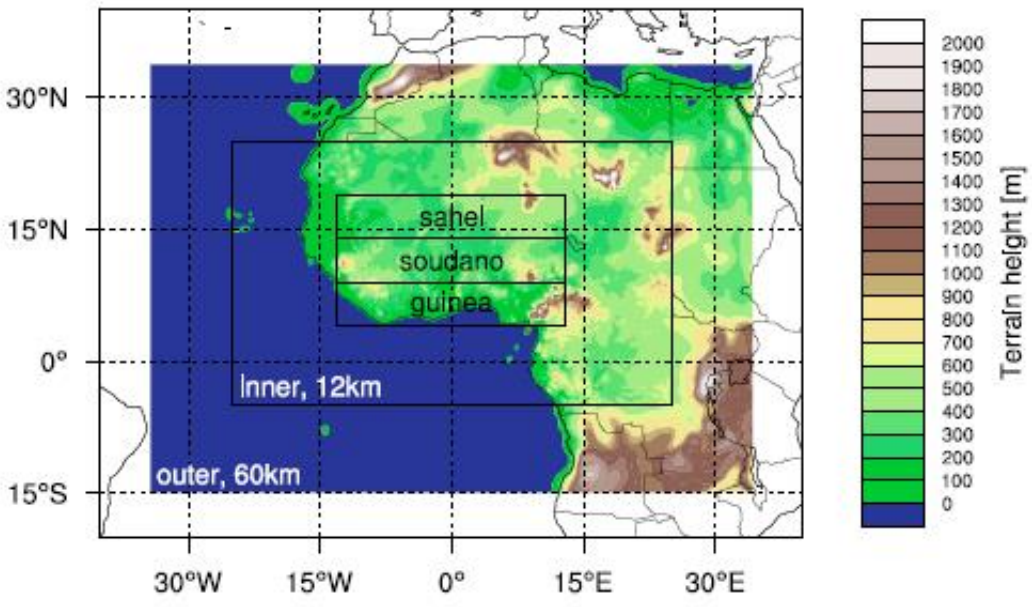

Figure 10: Nested domain configuration with 60 km and, 12 km. Also shown are three distinct agro-climatic regions used in the analysis make the agro-climatic regions a separate diagram (Heinzeller et al.,2017).

3-5 Method:

Three-hourly data of shortwave surface downward diffuse radiation (*swddif*), shortwave surface downward direct radiation (*swddir*) and surface Temperature (*ts*) were obtained from the 12km horizontal resolution Weather Research and Forecasting (WRF) Model simulations from https://cera-www.dkrz.de/WDCC/ui/Project.jsp?acronym=WASCAL.WRF was forced by the coupled Model Inter-Comparison Project Phase 5 (CMIP5) and ERA-INT as control experiment. Data from 1979-2006 for historical and control were used in this study. Then for selected climate change scenarios (RCP 4.5), over the period 2019-2050 and 2069-2100 were used. The changes in the parameters were tested for statistical significance.

3-6 Analysis Procedure:

From the three-hourly data obtained, the monthly mean of temperature, shortwave surface downward diffuse, and shortwave surface direct radiation were computed. Monthly and yearly mean for solar radiation and temperature were used to conduct this study.

The historical experiment was conducted by: simulations of WRF12KM-GFDLESM, WRF12KM-HADGEM2, WRF12KM-MPI and the control experiment was conducted by WRF12KM-ERA-INT.

First of all, monthly mean data (*swddir, swddif, ts*) obtained from the three Global climate model historical simulations (WRF12KM-GFDLESM, WRF12KM-HADGEM2, WRF12KM-MPI) for the period 1979-2006 were compared to the control simulation (WRF12KM-ERA-INT) for the same period. The objective was to identify which of those three model simulations best correlated with the control simulation. Taylor Diagrams were plotted for all the variables over the three regions of West Africa (Sahel, Savanna, Guinea-Cost) with the R software.

Taylor diagrams (Taylor, 2001) provide a way of graphically summarizing how closely a pattern (or a set of patterns) matches observations. The similarity between two patterns is quantified in terms of their correlation, their centered root-mean-square difference and the amplitude of their variations (represented by their standard deviations). These diagrams are especially useful in

evaluating multiple aspects of complex models or in gauging the relative skill of many different models (e.g., IPCC, 2001).

The next step was to analyze the trend and variability of *swddir*, *swddif*, and ts over Bamako and Mopti and to show the future evolution of *swddir*, swddif, *ts* using rcp4.5 scenarios for the period of 2019-2050 and 2079-2100. Then compare the two areas and find which will be suitable for PV technologies. The NCL software was used to conduct this part.

3.6.1 Statistics:

Given a "test" field (*f*) and a reference field (*r*), the formulas for calculating the correlation coefficient (*R*), the centered RMS difference (*E*'), and the standard deviations of the "test" field (*σf*) and the reference field (*σr*) are given below:

$$R = \frac{\frac{1}{N}\sum_{n=1}^{N}\left(f_n - \bar{f}\right)\left(r_n - \bar{r}\right)}{\sigma_f \sigma_r} \quad \textbf{(3.3)}$$

$$E'^2 = \frac{1}{N}\sum_{n=1}^{N}\left[\left(f_n - \bar{f}\right) - \left(r_n - \bar{r}\right)\right]^2 \quad (3.4)$$

$$\sigma_f^2 = \frac{1}{N}\sum_{n=1}^{N}\left(f_n - \bar{f}\right)^2 \quad (3.5)$$

$$\sigma_r^2 = \frac{1}{N}\sum_{n=1}^{N}\left(r_n - \bar{r}\right)^2 \quad (3.6)$$

where the overall mean of a field is indicated by an overbar. In the case of a time-independent field, the sum is computed over all grid cells. For the typical spatial grid, the grid cell area is not uniform, so each grid cell must be weighted by the fraction of the total area represented by that

grid cell. In the case of a time varying field, the sum is a double-sum computed over all grid cells and all-time samples.

-Linear regression the trend analysis for significance test:

Regression analysis is a process of predicting the values of one response or dependent variable from known values of a predictor or independent variable. The strength of the relationship between the dependent and independent variables is often clear when a scatter plot is drawn. A least squares line can be fitted to describe the relationship. The strength of the relationship between the dependent and independent variables is determined by the coefficient of determination, *R*-square, which measures the reproducibility of the response variable from the predictor values. The *R*-square values range from 0 (for no relationship) to 1 (for very strong relationship). The relationship between the response variable, and the predictor variable x is summarized by a linear equation y = bx + a, where b and a are respectively the slope of the least squares regression line and its intercept on the y axis. Normal distribution is a requirement for optimal regression analysis. Where the data is other than normal, a transformation scheme is applied to rectify it. A log transformation is frequently used to correct data that is not normally distributed.

$$y_i = \alpha + \beta * x_i + \varepsilon_i \tag{3.7}$$

Where Epsilon describes the random component of the linear relationship between x and y.

The probability value (p-value) is the most important concept of statistical significance and therefore an applicability of the results of a (trend) test.

The p-value represents the probability of an error when considering the real value of estimated parameter differs from the computed (or static) one, e.g., that the zero hypothesis holds although we considered the alternative one. Usually, if the p-value is under 5%, we accept the alternative hypothesis, because the risk of its invalidity is relatively low.

Chapter 4

Results and Discussion:

In order to identify which of the GCMs is most suitable for driving the WRF12km model, the WRF-GCM driven (i.e. GFDL, MPI, HADGEM) simulations were compared to the WRF-ERA-Interim driven simulation over the Guinea-Coast, Sahel and Savanna of West Africa. The GCM that drives WRF to best simulate shortwave-surface-downward-diffuse-irradiance, shortwave-surface-downward-direct-irradiance and surface temperature over these regions was identified by using the correlation, root mean square error, and standard deviation statistics. Each GCM used to drive WRF at 12km horizontal resolution was compared with the ERA-Interim driven simulation.

The projection, trend and variability of surface temperature, shortwave-surface-downward-diffuse-irradiance and shortwave-surface-downward-direct-irradiance obtained from WRF 12 KM simulation using the best forced GCM over the Sahel was examined. The projection is from RCP4.5 scenario and cover the middle of the twenty first century (2019-2050) and the end of twenty first century (2069-2100) for Bamako and Mopti.

4.1 Evaluation of WRF12km output:

The correlation R, standard deviation (σ), and root mean square difference RMSE (E') calculated in the equations (3.3,3.4,3.5,3.6) are used to assess how well the forced GCMs can simulate long term (1980–2005) shortwave-surface-downward-diffuse-irradiance (*swddif*), shortwave-surface-downward-direct-irradiance (*swddir*) and long term (1979-2006) surface temperature(*ts*). Only GCMs with high correlation and low RMSE were selected in this work.

From the table 10 (a) and figure 11-a (i.e Guines_Coast), WRF simulations forced by all of the three GCMs overestimated shortwave surface downward diffuse irradiance over the Guinea coast regions, but among the three models WRF12 km run by MPI is found to have the highest correlation and lowest RMSE followed by GFDL so MPI was selected.

From the table 10 (b) and figure11-b (i.e Sahel), all the forced GCMs estimated well *swddif* over the Sahel regions but of the three models MPI has the highest correlation and lowest RMSE.

From the table 10 (c) and figure-11-c (Savanna), MPI and HADGEM were found to estimate swddif over the Savanna regions reasonably well, while GFDL overestimated the *swddif*. Of the three forcing GCMs, MPI was selected.

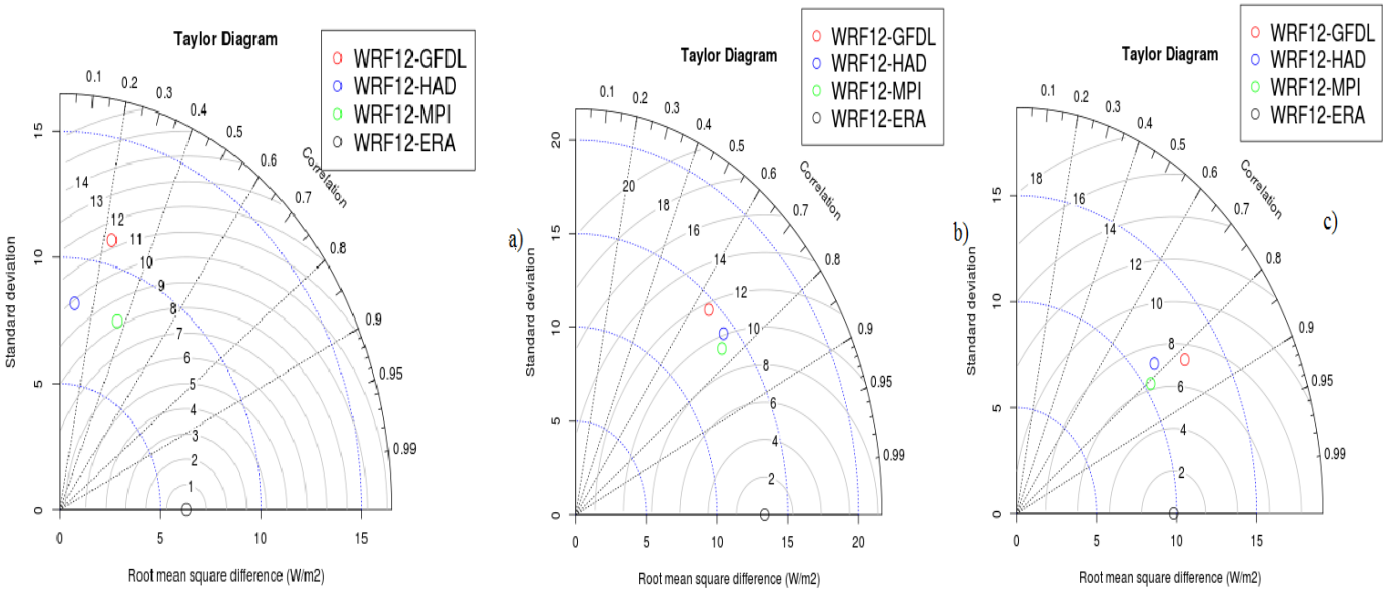

Figure 11: The Taylor's Diagram for the shortwave surface downward diffuse irradiance over the three regions with ERA-interim as reference (Guineas-Coast a), Sahel b), Savanna c)).

Table 10: The values of R, σ and RMSE for shortwave surface downward diffuse irradiance over the (a) Guinea Coast; (b) Sahel and (c) Savanna regions.

(a) Guinea Coast

Shortwave-surface –Downward- diffuse-irradiance			
	σ	R	RMSE
WRF12GFDLESM_hist	11	0.25	11.2
WRF12HADGEM_hist.	8	0.15	9.9
WRF12-MPIESM_hist.	8	0.38	8.1
ERA-Interim	6	1	0

.

(b) Sahel

WRF12GFDLESM_hist	14.7	0.65	11.8
WRF12HADGEM_hist.	14.6	0.75	10
WRF12-MPIESM_hist.	14	0.78	9.7
ERA-Interim	14	1	0

© Savanna

WRF12GFDLESM_hist	13	0.83	7.2
WRF12HADGEM2_hist.	11	0.75	7.5
WRF12-MPIESM_hist	10.2	0.82	6.2
ERA-Interim	9.9	1	0

From table 11(a) (i.e. Guineas_coast) and figure12-a only WRF12 run by MPI gave a better estimate of *swddir* over the Guinea-coast but with a correlation inferior to HADGEM. GFDL overestimated *swddir* in Guinea-coast. MPI and HADGEM had the highest correlation and lowest RMSE and were thus selected.

Table11(b) and figure12-b (i.e Sahel) show that: all the forced GCMs underestimated swddir over the Sahel regions but of the three models MPI has the highest correlation and lowest RMSE.

From table11 © and figure 12-c (i.e Savanna) WRF12 km run by MPI and GFDL underestimated *swddir* in this region while HADGEM overestimated. However, MPI has been selected with the highest correlation of 0.77 and lowest root mean square difference of 15W/m2 and Standard Deviation of 20.

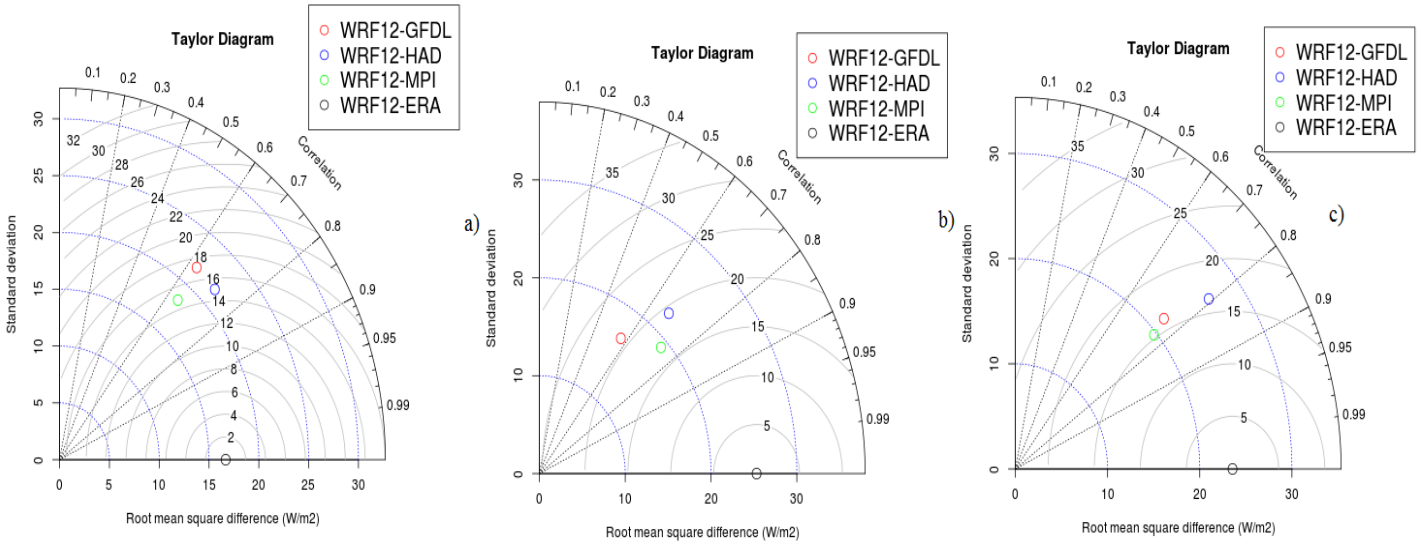

Figure 12:The Taylor's Diagram for the shortwave surface downward direct irradiance over the three regions with ERA-interim as reference (Guinea-Coast a), Sahel b), Savanna c)).

Table 11: The values of R, σ and RMSE for shortwave surface downward direct irradiance over the (a) Guinea Coast; (b) Sahel and (c) Savanna regions.

(a) Guinea Coast

Shortwave-surface –Downward- direct-irradiance			
	σ	R	RMSE
WRF12GFDLESM_hist	21	0.63	17.5
WRF12HADGEM_hist.	22	0.75	15
WRF12-MPIESM_hist.	18	0.65	15
ERA-Interim	17	1	0

(b) Sahel

	σ	R	RMSE
WRF12GFDLESM_hist	13	0.59	21
WRF12HADGEM_hist.	21	0.7	19
WRF12-MPIESM_hist.	19	0.75	17
ERA-Interim	26	1	0

(c) SAVANNA

	σ	R	RMSE
WRF12GFDLESM_hist	22	0.75	17
WRF12HADGEM_hist.	28	0.8	17
WRF12-MPIESM_hist.	20	0.77	15
ERA-Interim	24	1	0

From the table 12(a) and figure13-a (i.e Guinea _Coast), WRF12km run by GFDL gave a good estimate of *ts* while that run by MPI and HADGEM underestimated. MPI was selected with the highest correlation of 0.75 and lowest root mean square difference equal to 0.73°C and Standard Deviation of 0.7.

From the table 12 (b) and figure13-b (i.e Sahel) all the GCMs estimated *ts* well. MPI and HADGEM were selected over this region.

From the table 12 © and figure13-c (i.e Savanna), HADGEM and GFDL overestimated *ts* while MPI estimated it reasonably well. MPI was selected with the highest correlation and lowest root mean square difference over this region.

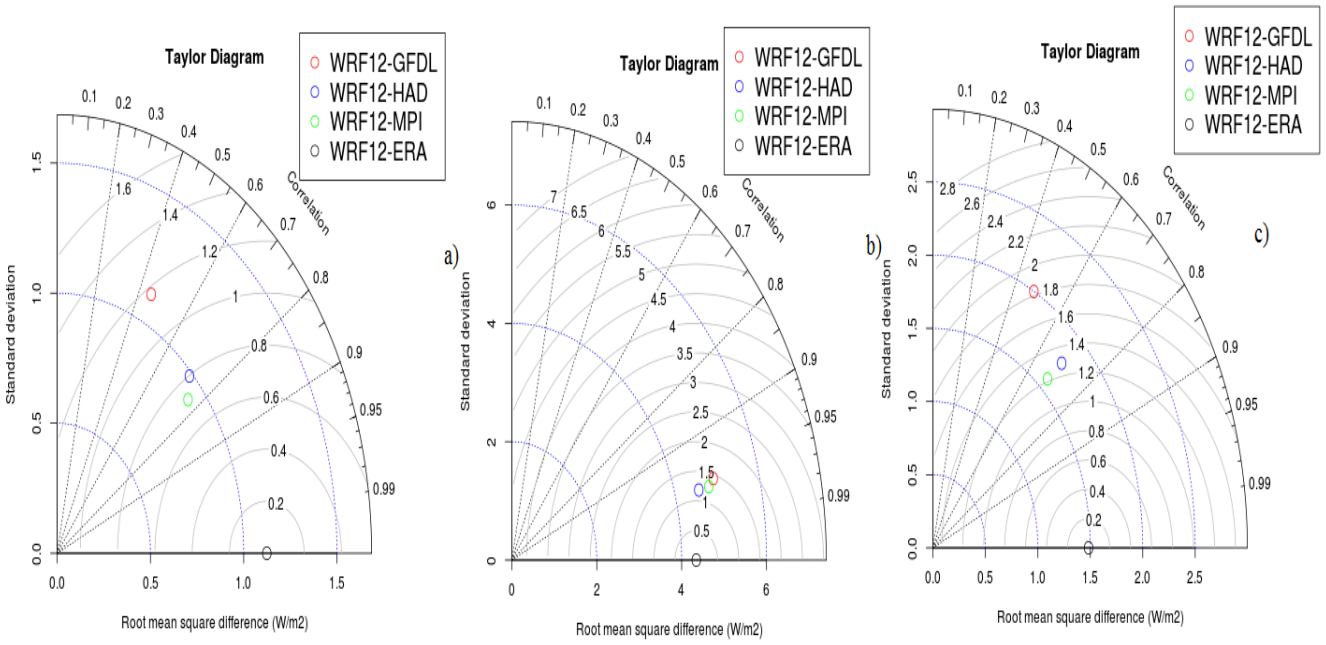

Figure 13: The Taylor's Diagram for the surface temperature over the three regions with ERA-interim as reference (Guinea-Coast a), Sahel b), Savanna c)).

Table 12: The values of R, σ and RMSE for surface temperature over the (a) Guinea Coast; (b) Sahel and (c) Savanna regions.

(a) Guinea Coast

Surface Temperature			
	σ	R	RMSE
WRF12GFDLESM_hist	1.15	0.45	1.18
WRF12HADGEM_hist.	1.0	0.7	0.8
WRF12-MPIESM_hist.	0.7	0.75	0.73
ERA-Interim	1.16	1	0

(b) Sahel

	σ	R	RMSE
WRF12GFDLESM_hist	5	0.95	1.5
WRF12HADGEM_hist.	4.5	0.96	1.25
WRF12-MPIESM_hist.	4.8	0.96	1.26
ERA-Interim	4.3	1	0

© Savanna

	σ	R	RMSE
WRF12GFDLESM_hist	2.0	0.5	1.8
WRF12HADGEM_hist.	1.8	0.7	1.3
WRF12-MPIESM_hist.	1.6	0.7	1.2
ERA-Interim	1.5	1	0

4.2 Variability and trend of projected solar radiation over Bamako and Mopti:

4.2.1 Variability and trend of projected shortwave-surface-downward-diffuse-irradiance over Bamako and Mopti:

Figure 14, shows the intra-annual plots of shortwave-surface-downward-diffuse-irradiance over Bamako and Mopti from, the reference period (1979-2005) to near future (2019-2050) and the far future (2069-2100) under RCP4.5 scenario.

For the period of (2019-2050), compared to the reference years (1979-2005) there was a decrease in *swddif* for the months (February, March, April, June, July, October and December) for Bamako and (March, April, June, July, August, October and December) for Mopti and an increase during the months of (May, August, September and November) for Bamako and during the months of (February ,May, and November) for Mopti (figure14, e, f) The increase in diffuse irradiance during the month of May for both Bamako and Mopti, may be due to the fact that, during certain years, the rainy season starts in May in the Sahel region. The increase in October, November, February

could be due to increased dust in the environment caused by the harmattan winds during those months. The August and September increase could be due to increased cloud cover because this period in Mali is rainy season. Two peaks are clearly observed for both Bamako and Mopti. In Bamako the peaks are observed during the months of February and July, while in Mopti the peaks are observed during the months of March and July. The peak for Bamako is almost the same compared to the reference years and for Mopti it decreases a little than the reference years (figure14, a, b). However, increase in diffuse irradiation is higher in Bamako than Mopti. It is up to +2.5W/m2 for Bamako and +1W/m2 for Mopti. Both maximum values are observed in the month of May (figure14, e, f). The minimum values are observed in the months of October and November for Bamako and October for Mopti (figure14, a, b).

During the period 2019-2050, a large decrease in diffuse irradiance, -3W/m2, is observed during the month of June for Bamako and during the month of September (-3.5W/m^2) for Mopti. These may be due to less cloud cover n in those months (figure14, e, f).

At the end of the 21st century, there was a general decrease (compared to the reference years) in swddif over both cities, except for May and November for Bamako and May, October and November for Mopti where there were increases. This increase in diffuse irradiance during the month of May, may be due to the fact that in some years the rainy season start in May in the Sahel regions. The increases in October and November could be due to increased dust in the environment caused by the harmattan winds (figure14, g, h). Two peaks were clearly observed over both cities. These were in February and July for Bamako, and March and July for Mopti. The peaks decreased over both cities with respect to the reference years (1979-2005) (figure14, c, d). However, the magnitude of the increase in diffuse irradiation was higher in Bamako than Mopti, although it was observed in the month of May over both cities. The values were up to +3.5W/m2 for Bamako and +1.75W/m2 for Mopti (figure14, g, h). The minima were observed in the months of October and November for Bamako and for Mopti in the month of October (figure14, c, d). Large negative anomalies in diffuse irradiance were observed during the month of July over both cities. A value of -2.75W/m2 for Bamako -4W/m2 for Mopti. This may be due to less cloud cover in those months (figure14, g, h).

Thus, it's has been observed for both of the periods, (i.e. (2019-2050) and (2069-2100)), that the increase in diffuse irradiance is higher in Bamako than Mopti. This is due to the fact that Bamako

is the capital and has more industries. Thus, air pollution is higher there than the desert parts of the country. Polluted air quality contributes to regional aerosol effects (IPPCC Fourth assessment report ,2007).

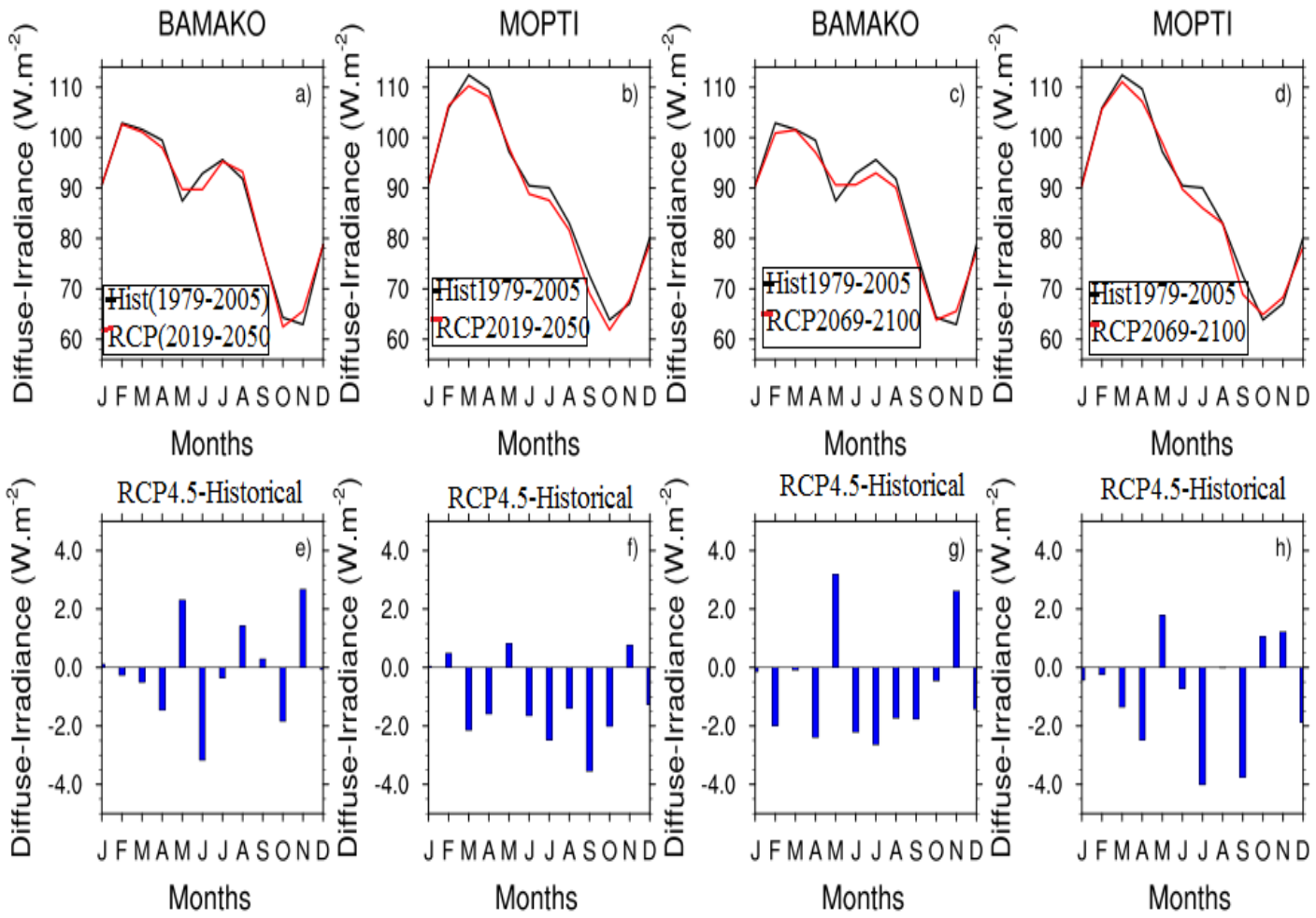

Figure 14:Time series of shortwave downward diffuse irradiance for the reference period to the near future and far future (a) rcp4.52019-2050 and historical 1979-2005 for Bamako, (b) rcp4.52019-2050 and historical 1979-2005 for Mopti, (c) rcp4.5 2069-2100 and historical 1979-

2005 for Bamako, (d) rcp4.52069-2100 and historical 1979-2005 for Mopti, (e) rcp4.5 2019-2050 minus historical1979-2005 for Bamako, (f) rcp4.5 2019-2050 minus historical1979-2005 for Mopti, (g) rcp4.5 2069-2050 minus historical1979-2005 for Bamako, (h) rcp4.5 2019-2050 minus historical1979-2005 for Mopti.

From figure15 and table13 it was oberved a decreasing trend in *swddif* during the references period (1979-2005) and an increasing trend during the near future and far future for both Bamako and Mopti. These increasing trends may be due to the enhanced greenhouse gases in the atmosphere. Greenhouse gases absorb some of solar radiation in the atmosphere and the remains are reflected in the earth surface as diffuse radiation. For Bamako, analysis shows a negative trend for the reference period. This negative trend is not statistically significant at the 68% confidence level. A positive trend is observed for both near and far future, this positive trend is statistically significant and at the 98% confidence level for the near future and it is not statistically significant at the 90% confidence level for the far future. For Mopti, analysis shows a negative trend for the reference period. This negative trend is not statistically significant at the 75% confidence level. A positive trend is observed for both near and far future, this positive trend is statistically significant at the 99% confidence level for the near future and at the 99% confidence level for the far future.

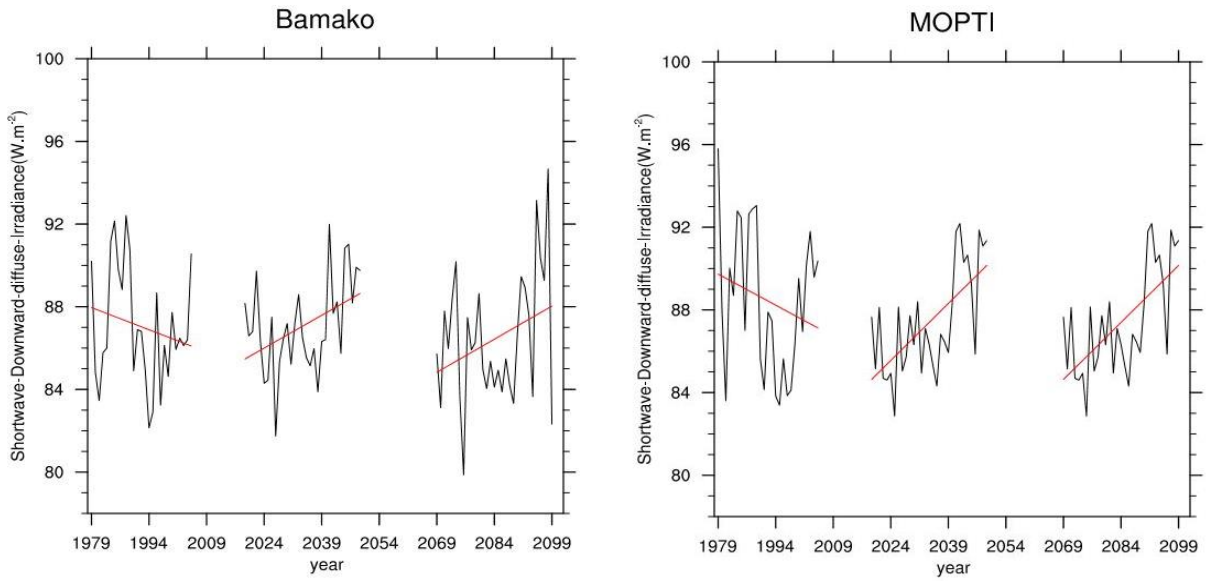

Figure 15: Time series of the inter-annual evolution of shortwave downward diffuse irradiance for the reference period to the near future and far future over left Bamako and right Mopti under RCP4.5 Scenario.

Table 13: The values of regression coefficient and probability values for swddif

	Period	Reg-coefficient	P-Value
Bamako	Historical (1979-2005)	-0.07138795	0.325856
	RCP4.5(2019-2050)	0.1057256	0.01721655
	RCP4.5(2069-2100)	0.1068037	0.09556841
Mopti	Historical (1979-2005)	0.100213	0.259085
	RCP4.5(2019-2050)	0.1837915	0.00007983064
	RCP4.5(2069-2100)	0.1837915	0.00007983064

4.2.2 Variability and trend of projected shortwave-surface-downward-direct-irradiance over Bamako and Mopti:

Figure 16, shows the intra-annual plots of shortwave-surface-downward-direct-irradiance over Bamako and Mopti from, the reference period (1979-2005) to near future (2019-2050) and the far future (2069-2100) for RCP4.5 scenario.

For the period of (2019-2050), compared to the reference years (1979-2005) a decrease in *swddir* was observed for almost the months of the year for both Bamako and Mopti and an increase during the months of (April, July, September, October) for both Bamako and Mopti, this increase in July and September could be due to more cloud cover (figure16 e, f). Two peaks were clearly observed in May and October over both localities. The peak of May is lower compared to the reference years while in October it's almost the same (figure16, a, b). However, increase in direct irradiation is almost the same in Bamako and Mopti. The value is up to +2W/m2 observed in the month of July for both Bamako and Mopti compared to the reference years (figure16, e, f). The minimum is

observed in the months of August for both Bamako and Mopti (figure16, a, b). A large decrease is observed in the month of May for both localities and is up to -10W/m^2. This could be due to increased cloud cover (figure16, e, f).

For the end of 21st century, a decrease in *swddir* was observed for ten out of the twelve months of year for both Bamako and Mopti. There were increases during the months of July and June for both Bamako and Mopti (figure16, g, h). Two peaks are clearly observed during the month of May and October for both localities. The peak in May is almost the same compared to the reference years but in October it is less (figure16, c, d). However, increase in direct irradiation is the same for Bamako and Mopti. The magnitude is up to +6W/m2 observed in the month of July for both Bamako and Mopti (figure16, g, h). The minimum was observed in the month of August for both Bamako and Mopti (figure16, c, d). A large decrease is observed in the month of May for both localities. The value is -13.5W/m2. This could be due to increased cloud cover (figure16, g, h).

Thus, it was observed that the increase in direct irradiance is almost the same in Bamako and Mopti. For both periods (i.e. (2019-2050) and (2069-2100)).

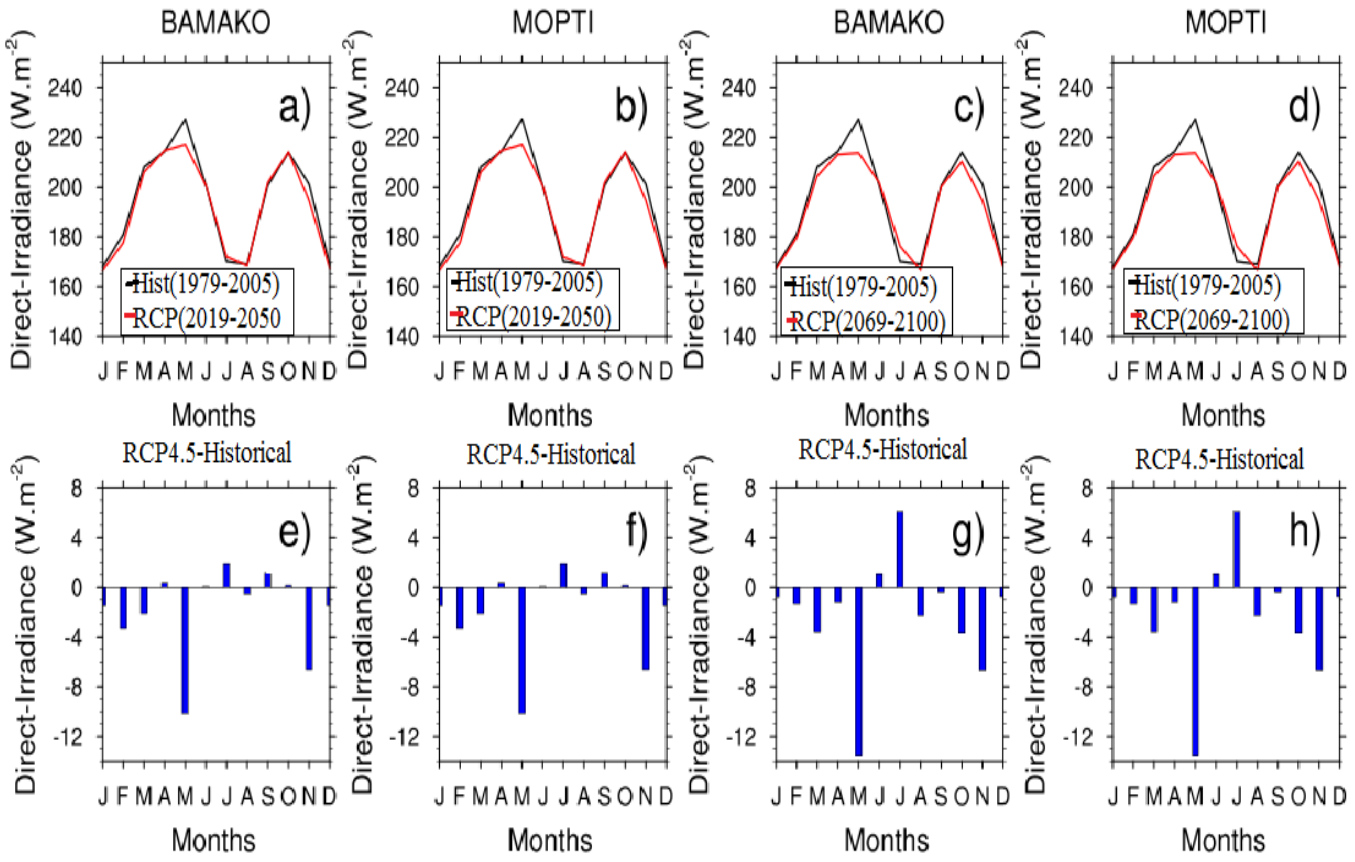

Figure 16: Time series of the inter-annual evolution of shortwave downward direct irradiance for the reference period to the near future and far future over Bamako and Mopti under RCP4.5 Scenario future (a) rcp4.52019-2050 and historical 1979-2005 for Bamako, (b) rcp4.52019-2050 and historical 1979-2005 for Mopti, (c) rcp4.5 2069-2100 and historical 1979-2005 for Bamako, (d) rcp4.52069-2100 and historical 1979-2005 for Mopti, (e) rcp4.5 2019-2050 minus historical1979-2005 for Bamako, (f) rcp4.5 2019-2050 minus historical1979-2005 for Mopti, (g) rcp4.5 2069-2050 minus historical1979-2005 for Bamako, (h) rcp4.5 2019-2050 minus historical1979-2005 for Mopti.

Figure 17 and table 14 show an increase of *swddir* during the reference period (1979-2005), near future and far future for Bamako. For Mopti, there was an increase of *swddir* during the reference period (1979-2005), decrease during the near future and an increase for the far future. The analysis for Bamako shows a positive trend for the reference period. This positive trend is not statistically significant at the 22% confidence level. A positive trend is observed for both near and far future, this positive trend is not statistically significant at the 88% confidence level for the near future and

at the 69% confidence level for the far future. For Mopti, analysis shows a positive trend for the reference period, this positive trend is not statistically significant.

A negative trend is observed for near future. This negative trend is not statistically significant at the 87% confidence level. A positive trend is observed for the far future. This positive trend is not statistically significant at the 1% confidence level.

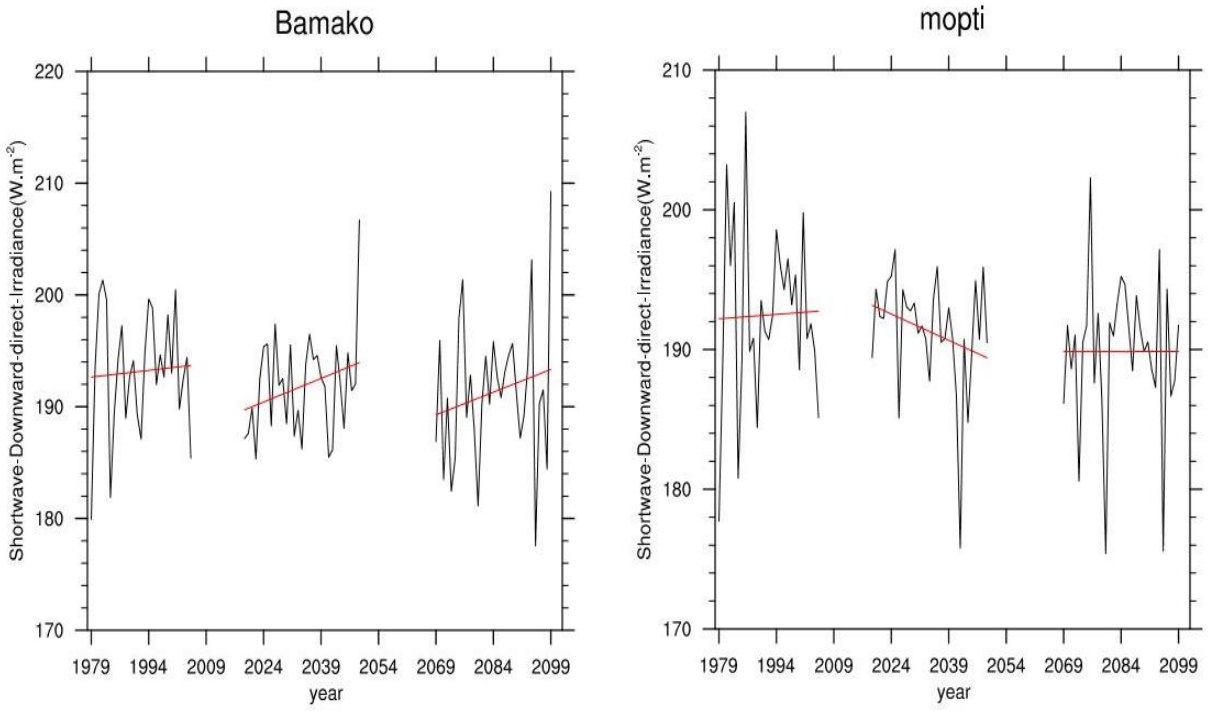

Figure 17: Time series of the inter-annual evolution of shortwave downward direct irradiance for the reference period to the near future and far future over left Bamako and right Mopti under RCP4.5 Scenario.

Table 14: The values of regression coefficient and probability values for swddir.

	Period	Reg-coefficient	P-Value
Bamako	Historical (1979-2005)	0.03996868	0.775968
	RCP4.5(2019-2050)	01409122	01206618
	RCP4.5(2069-2100)	0.1352804	0.3100502

Mopti	Historical (1979-2005)	0.02113148	0.897008
	RCP4.5(2019-2050)	-0.125141	0.1368464
	RCP4.5(2069-2100)	0.0002045847	0.9985036

4.3 Variability and trend of projected surface Temperature over Bamako and Mopti:

Figure 18 shows the intra-annual plots of surface Temperature over Bamako and Mopti from, the reference period (1979-2005) to near future (2019-2050) and the far future (2069-2100) for RCP4.5 scenario.

A continuous increase in surface temperature is clearly observed for the near and far future over both Bamako and Mopti (figure 18, a, b, c, d, e, f, g, h). The peaks over both localities are observed in May, September, October, and November. A high augmentation is observed during the month of February for both near and far future (figure 18, a, c, d, e, f, g, h).

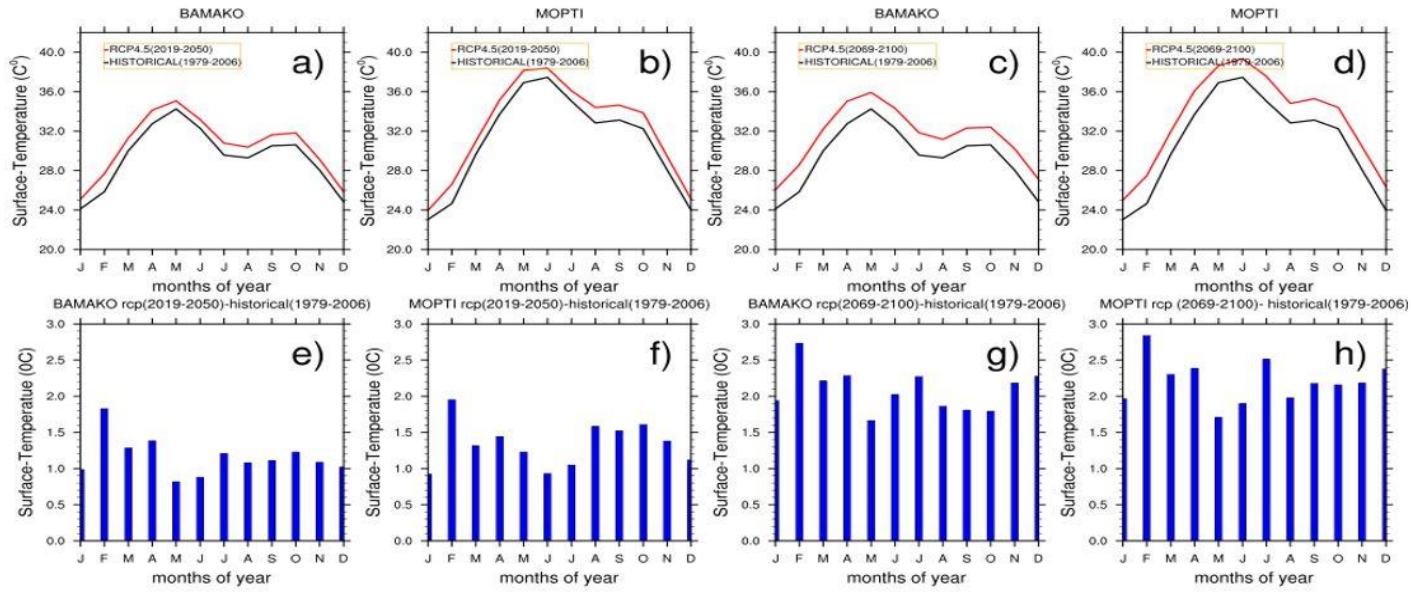

Figure 18: Time series of the inter-annual evolution of surface Temperature for the reference period to the near future and far future over Bamako and Mopti under RCP4.5 Scenario future (a) rcp4.52019-2050 and historical 1979-2005 for Bamako, (b) rcp4.52019-2050 and historical 1979-

2005 for Mopti, (c) rcp4.5 2069-2100 and historical 1979-2005 for Bamako, (d) rcp4.52069-2100 and historical 1979-2005 for Mopti, (e) rcp4.5 2019-2050 minus historical1979-2005 for Bamako, (f) rcp4.5 2019-2050 minus historical1979-2005 for Mopti, (g) rcp4.5 2069-2050 minus historical1979-2005 for Bamako, (h) rcp4.5 2019-2050 minus historical1979-2005 for Mopti.

The time series of the inter-annual evolution of surface Temperature for the reference period to the near future and far future over Bamako and Mopti under RCP4.5 Scenario is shown in figure 19. From figure 19 and table 15 an increase of *ts* during the reference period (1979-2005), near and far future for both Bamako and Mopti. The Bamako analysis shows a positive trend for the reference period. This positive trend is statistically significant and at the 99% confidence level. A positive trend is observed for both near and far future. This positive trend is statistically significant at the 99% confidence level for the near future and is not statistically significant at the 45% confidence level for the far future. For Mopti, the analysis shows a positive trend for the reference period, this positive trend is not statistically significant at the78% confidence level. A positive is observed for both near and far future, this positive trend is statistically significant at the 98% level for the near future and not statistically significant at the 39% confidence level for the far future.

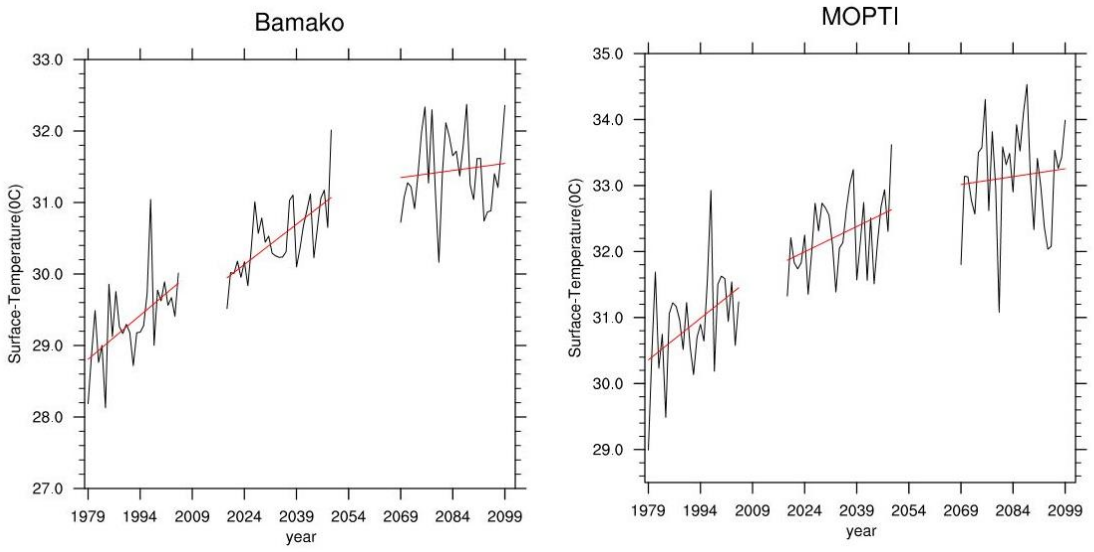

Figure 19: Time series of the inter-annual evolution of surface temperature for the reference period to the near future and far future over left Bamako and (b) right Mopti under RCP4.5 Scenario.

Table 15: The values of regression coefficient and probability values for surface temperature.

		R	P value
Bamako	Historical (1979-2005)	0.04098377	0.002392889
	RCP4.5(2019-2050)	0.03746178	0.00004
	RCP4.5(2069-2100)	0.00662368	0.55506905
Mopti	Historical (1979-2005)	0.04204715	0.02295242
	RCP4.5(2019-2050)	0.0255559	0.02443316
	RCP4.5(2069-2100)	0.0079293	0.6146144

Chapter 5

Conclusions and Future Work

5.1 General Conclusions:

It is well admitted that climate variability and change will have direct impact on energy infrastructure and technology as well as on energy supply and demand. Changes in mean climate parameters such as surface temperature and solar radiation will have impacts on some renewable technologies including PV modules.

In this study, the impact of climate change on solar energy potential over West-Africa was investigated with a focus on MALI.

The WRF-12km output was evaluated and Taylor diagrams were plotted Over Guinea-coast, Sahel, Savanna regions of West-Africa for the parameters, shortwave downward diffuse radiation (swddif), shortwave downward direct radiation (*swddir)* and surface temperature (*ts*). The aim was to identify the best forcing GCM for WRF over these regions with regards to the three parameters mentioned earlier. Thus, the best forcing GCM over the Sahel region was used to analyze the trend and variability of the parameters over Bamako and Mopti. Analysis showed that all the three forcing GCMs (GFDL, HADGEM, MPI) overestimated *swddif* over the Guinea coast, but MPI was found to have the highest correlation of 0.38 and the lowest root-mean-square- difference of $8.1Wm^2$ compared to the reference (ERA-Interim). Over the Sahel region all the three forcing GCMs estimated *swddif* reasonably well, but MPI was found to have the highest correlation of 0.78 and lowest root-mean-square-error of 9.7W/m2 compared to the reference. Over Savanna region MPI and HAD-GEM were found to estimate the *swddif* reasonably well, *while* GFDL overestimated. MPI had the highest correlation 0.82 and lowest root-mean-square-error of 6.2W/m2 compared to the reference.

For *swddir,* analysis showed that only MPI estimated it reasonably well in the Guinea coast region, while HAD-GEM and GFDL overestimated it. MPI and HAD-GEM were found to have the highest correlation of 0.65 and 0.75 respectively. The lowest root-mean-square-error of $15W/m^2$ was obtained for both compared to the reference. Over the Sahel region, all the forcing GCMs underestimated *swddir,* but of the three models, MPI was found to have the highest correlation of

0.75 and the lowest root-mean-square-error 17W/m^2. Over Savanna, MPI and GFDL underestimated *swddir* while HAD-GEM overestimated compared to the reference was find to have the highest correlation 0.77 and the lowest root-mean-square-error 15W/m2.

The analysis for *ts* showed that GFDL estimated reasonably well while HAD-GEM and MPI underestimated over Guinea coast. MPI was found to have the highest correlation of 0.75 and the lowest root-mean-square-error 0.73 °C for Guinea Coast. Over the Sahel region, all the three forcing GCMs estimated ts well. *MPI* and HADGEM were found to have the highest correlation of 0.96. and the lowest root-mean-square-error of 1.25°C for HADGEM and 1.26°C for MPI compared to the reference. Over the Savanna region, HADGEM and GFDL overestimated *ts* while MPI estimated it well. MPI was found to have the highest correlation of 0.7 and the lowest root-mean-square-error of 1.2 °C compared to the reference.

Analysis showed that in all the three regions of West Africa, WRF12km driven by MPI has the highest correlation and the lowest root-mean-square-error followed by HADGEM compared to the reference.

In terms of trend and variability of *swddif, swddir* and *ts*, the analysis showed that the increase in *swddif* is more significant in the near and far future in Bamako than Mopti. For the near future, a value of +2.2W/m2 for Bamako and and +1W/m2 for Mopti were both observed in May. For the far future, a value of +3.5W/m2 for Bamako and +1.75W/m2 for Mopti were observed in May. However, increase in *swddir* is almost the same for Bamako and Mopti, there is an increase of temperature over both localities and it's more significant in Mopti than Bamako.

Thus, based on the three parameters used in this study, the locality of Mopti will be more suitable for implementation of solar energy panels to satisfy the energy needs in Mali.

Regarding the siting of the solar panels (or solar farms), there are additional factors that have to be considered before a decision is made. For instance, land cover, the current and projected cost of land, the layout of the national grid lines, the intended plans of the government regarding expansion of the national grid. Even with climatic factors, grass minimum or soil temperature, wind and the maximum radiation also need to be considered.

5.2Future Work:

This study was limited to simulating the impact of climate change on solar energy potential over Mali by analyzing surface temperature and solar radiation. Climate change impacts on photovoltaic systems could be further investigated looking at other climate parameters that have notable impact on PV energy output, for instance wind. The forced convection due to wind removes heat from the module and consequently decreases its temperature, extreme events, and the topography.

REFERENCES:

Abdou-Ali,2016 (ADVANCED STATISTICS&GEOSTATISTICS.pdf).

Badger, Jake; Kamissoko, Famakan; Olander Rasmussen, Mads; Larsen, Søren Ejling; Guidon, Nicolas; Hansen, Lars Boye; Dewilde, Luc; Nørgård, Per Bromand; Nygaard, Ivan, Estimation of wind and solar resources in Mali,2012.

Charles Fant , C. Adam Schlosser, Kenneth Strzepek 2017 The impact of climate change on wind and solar resources in southern Africa.

Denis, B., Laprise, R., Caya, D. and Coˆte, J. 2002. Downscaling ability of one-way nested regional climate models: the Big-Brother Experiment, *Climate Dynamics*, 18, 627–646. doi:10.1007/s00382-001-0201-0.

Davies, H. C.: Limitations of Some Common Lateral Boundary Schemes used in Regional NWP Models, Monthly Weather Review, 111,20 1002–1012, https://doi.org/10.1175/1520-0493(1983)111<1002:LOSCLB>2.0.CO;2, 1983.

Dieng, D., Smiatek, G., Bliefernicht, J., Heinzeller, D., Sarr, A., Gaye, A. T., and Kunstmann, H.: Evaluation of the COSMOCLM high-resolution climate simulations over West Africa, Journal of Geophysical Research: Atmospheres, 122, 1437–1455, https://doi.org/10.1002/2016JD025457, 2017.

Daniels, A.E., Morrison, J.F., Joyce, L.A., Crookston, N.L., Chen, S.C., and McNulty, S.G. 2012. Climate projections FAQ. Gen. Tech. Rep. RMRS-GTR-277WWW. Fort Collins, CO: U.S. Department of Agriculture, Forest Service, Rocky Mountain Research Station, 32 pp.

Dominikus Heinzeller1, Diarra Dieng1,2, Gerhard Smiatek1, Christiana Olusegun1, Cornelia Klein3, Ilse Hamann4, Seyni Salack5, and Harald Kunstmann1, essd-2017-93.pdf.ECOWAS Renewable Energy and Energy Efficiency Status Report, REN21, 2014.

Elguindi, N., Giorgi, F., and Turuncoglu, U.: Assessment of CMIP5 global model simulations over the subset of CORDEX domains used in the Phase I CREMA, Climatic Change, 125, 7–21, https://doi.org/10.1007/s10584-013-0935-9, 2014.

Endris, H.S., Omondi, P., Jain, S., Lennard, C., Hewitson, B., Chang'a, L., Awange, J.L., Dosio, A., Ketiem, P., Nikulin, G., Panitz, H.J., Büchner, M., Stordal, F. and Tazalika, L. 2013. Assessment of the Performance of CORDEX regional climate models in simulating east African rainfall. *J. Climate*, 26, 8453–8475.

Energy Information Administration (EIA), official energy statistics from U.S. government. History: International Energy Annual 2004 (May–July 2006), website www.eia.doe.gov/iea. Projections : EIA, International Information Outlook 2007.

Energy du Mali - Plan de Redressement de la Situation Financiere et Operationelle du Secteur de l'Electricité, March 2014.

http://www.edm-sa.com.ml/edmsa/chiffres.asp.

Eseoghone Larhwei Hobson, (2016) Mapping & assessment of existing clean energy mini-gridexperiences in West-Africa.

Gambian Ministry of Energy & Petroleum; National Focal Institution for Guinea-Bissau; IRENA; National Focal Institution for Nigeria; UNDP; ECREEE.

Giorgi,F.,Jones,C.,andAsrar,G.R.:Addressingclimateinformationneedsattheregionallevel:theCORDEXframework,Bulletin-World Meteorological Organization, 58, 175–183, 2009.

Harris, L. M. and Durran, D. R.: An Idealized Comparison of One-Way and Two-Way Grid Nesting, Monthly Weather Review, 138, 2174– 2187, https://doi.org/10.1175/2010MWR3080.1, 2010.

Hassan, Z., Shamsudin, S., Harun, S. 2013. Application of SDSM and LARS-WG for simulating and downscaling of rain-fall and temperature, *Theor Appl Climatol*, 116, 43–257. doi: 10.1007/s00704-013-0951-8.

Intergovernmental Panel on Climate Change Fourth Assessment Report Climate Change, 2007

International Renewable Energy Agency.

IPCC, 2001: Climate Change 2001: The Scientific Basis, Contribution of Working Group I to the Third Assessment Report of the Intergovernmental Panel on Climate Change [Houghton, J.T., Y. Ding, D.J. Griggs, M. Noguer, P.J. van der Linden, X. Dai, K. Maskell, and C.A. Johnson (eds.)]. Cambridge University Press, Cambridge, United Kingdom and New York, NY, USA, 881 pp. (see http://www.grida.no/climate/ipcc_tar/wg1/317.htm#fig84).

Intergovernmental Panel on Climate Change Data Distribution Centre;2012. <http://www.ipcc-data.org> [accessed September 2012.

Ioanna S. Panagea,1 Ioannis K. Tsanis,1,2 Aristeidis G. Koutroulis,1 and Manolis G. Grillakis1 2014 Climate Change Impact on Photovoltaic Energy Output: The Case of Greece.

Jose A. Ruiz-Arias, Christian A. Gueymard, Jimy Dudhia, David Pozo-Vazquez 2012.

Julian_Chen, 2011_Physics_of_Solar_Energy(book.org).

Klein, C., Heinzeller, D., Bliefernicht, J., and Kunstmann, H.: Variability of West African monsoon patterns generated by a WRF multiphysics ensemble, Climate Dynamics, https://doi.org/10.1007/s00382-015-2505-5, http://link.springer.com/10.1007/s00382-015-2505-5, 2015.

Leduc, M. and Laprise, R.: Regional climate model sensitivity to domain size, Climate Dynamics, 32,833–854,5https://doi.org/10.1007/s00382-008-0400-z,

http://link.springer.com/10.1007/s00382-008-0400-z, 2008.

Li, D.H.W., Yang, L., Lam, J.C., 2012. Impact of climate change on energy use in the built environment in different climate zones – A review. Energy 42 (1), 103–112.

Luis Martín Pomares, L. Ramírez Santigosa 2016 Solar radiation forecasting with WRF model in the Iberian Peninsula.

Martin Wild, Doris Folini, and Florian Henschel 2017(Impact of climate change on future concentrated solar power (CSP) production) https://doi.org/10.1063/1.4975562

Min, E., Hazeleger, W., Oldenborgh, G.J. and Sterl, A. 2013. Evaluation of trends in high temperature extremes in north-western Europe in regional climate models, *Environ. Res. Lett*., 8. doi:10.1088/1748-9326/8/1/014011.

MiguezMacho,G.,Stenchikov,G.L.,andRobock,A.:Spectralnudgingtoeliminatetheeffectsofdomain positionandgeometryinregional10 climate model simulations, Journal of Geophysical Research D: Atmospheres, 109, https://doi.org/10.1029/2003JD004495, 2004.

Meier, H.E.M., Höglund, A., Döscher, R., Andersson, H., Löptien, U. and Kjellström, E. 2011. Quality assessment of atmospheric surface fields over the Baltic Sea from an ensemble of regional climate model simulations with respect to ocean dynamics, *Oceanologia*, 53(1-TI), 193–227.

M. Wild, D. Folini, F. Henschel, N. Fischer and B. Müller, Solar Energy **116**, 12-24 (2015).

Nikulin, G., Jones, C., Kjellström, E., and Gbobaniyi, E.: The West African Monsoon simulated by global and regional climate models, in: EGU General Assembly 2013, held 7-12 April, 2013 in Vienna, Austria, vol. 15, p. 4581, EGU, http://meetingorganizer.copernicus.org/ EGU2013/EGU2013-4581.pdf, 2013.

Noble, E., Druyan, L., and Fulakeza, M.: The sensitivity of WRF daily summertime simulations over West Africa to alternative param-35 eterizations. Part I: african wave circulation., Monthly Weather Review, 142, 1588–1608, https://doi.org/10.1175/MWR-D-13-00194.1, 2014.

Otte, T. L.: The impact of nudging in the meteorological model for retrospective air quality simulations.PartIEvaluationagainstnationalobservationnetworks,JournalofAppliedMeteorologyan dClimatology,47,1853–1867,https://doi.org/10.1175/2007JAMC1790.1,2008.

Otte, T. L., Nolte, C. G., Otte, M. J., and Bowden, J. H.: Does nudging squelch the extremes in regional climate modeling?, Journal ofClimate, 25, 7046–7066, https://doi.org/10.1175/JCLI-D-12-00048.1, 2012.

Ohunakin, O.S., Adaramola, M.S., Oyewola, O.M., Fagbenle, R.O., 2013. Correlations for estimating solar radiation using sunshine hours and temperature measurement in Osogbo, Osun State, Nigeria. Front.Energy. http://dx.doi.org/10.1007/s11708-013-0241-2.

Ohunakin, O.S., Adaramola, M.S., Oyewola, O.M., Fagbenle, R.O., 2015. Solar radiation variability in Nigeria based on multiyear RegCM3 simulations. Renewable Energy 74, 195–207.

Pan, Z., Segal, M., Arritt, R.W., Takle, E.S., 2004. On the potential change in solar radiation over the US due to increases of atmospheric greenhouse gases. Renewable Energy 29, 1923–1928.

Pal, J.S., Giorgi, F., Bi, et al., 2007. The ICTP RegCM3 and RegCNET: Regional climate modeling for the developing world. Bull. Am. Meteorol. Soc. 88, 1395–1409. http://dx.doi.org/10.1175/BAMS-88-9- 1395.

Park, S.-H., Klemp, J. B., and Skamarock, W. C.: A Comparison of Mesh Refinement in the Global MPAS-A and WRF Models Using an
Idealized Normal-Mode Baroclinic Wave Simulation, Monthly Weather Review, 142, 3614–3634, 2014.

Pyrina, M., Hatzianastassiou, N., Matsoukas, C., Fotiadi, A., Papadimas, C.D., Pavlakis, K.G., Vardavas, I., 2013. Cloud effects on the solar and thermal radiation budgets of the Mediterranean basin. Atmos. Res. http://dx.doi.org/10.1016/j.atmosres.2013.11.009.

Roux, B. 2009. Ultra-high-resolution climate simulations over the Stellenbosch wine-producing region using a variable-resolution model. M.Sc. Thesis. University of Pretoria, Pretoria, South Africa. 96 pp.

Renewable Energy-Africa-MALI Country profile 2015.

Respectively, CFCA 50 billion and CFCA 20 billion - Task-Force - Rapport Provisoire - Perspectives énergetiques à court terme du réseau interconnecté - Recommandations pour le redressement de la situation financière et opérationnelle du secteur de l'électricité pour la période 2014-2020.

Rossow, W.B., Schiffer, R.A., 1999. Advances in understanding clouds from ISCCP. Bull. Am. Meteorol. Soc. 8, 2261–2287.

Seljom P, Rosenberg E, Fidje A, Haugen JE, Meir M, Rekstad J, et al. Modelling the effects of climate change on the energy system—a case study of Norway.
Energy policy. Elsevier; 2011.

Serge Dimitri Bazyomo , Agnidé Emmanuel Lawin ,Ousmane Coulibaly ,Dominik Wisser , and Abdoulaye Ouedraogo Forecasted Changes in West Africa Photovoltaic Energy Output by 2045 ,2016.

Tchotchou, L.A.D., Kamga, F.M., 2010. Sensitivity of the simulated African monsoon of summers 1993 and 1999 to convective parameterization schemes in RegCM3. Theor. Appl. Climatol. 100, 207–220.

United Nations' Sustainable Energy for All (SE4ALL).

Villegas, J.R., and Jarvis, A. 2010. Downscaling global circulation model outputs: the delta method. Decision and Policy Analysis Working Paper No. 1, Centro internacional de agricultura Tropical.

Vardavas, I.M., Taylor, F.W., 2011. Radiation and Climate: Atmospheric Energy Budget from Satellite Remote Sensing, International Series of Monographs on Physics 138. Oxford University Press, Oxford.

van Vuuren, D. P., Edmonds, J., Kainuma, M., Riahi, K., Thomson, A., Hibbard, K., Hurtt, G. C., Kram, T., Krey, V., Lamarque, J. F., Masui, T., Meinshausen, M., Nakicenovic, N., Smith, S. J., and Rose, S. K.: The representative concentration pathways: An overview, Climatic Change, 109, 5–31, https://doi.org/10.1007/s10584-011-0148-z, 2011.

von Storch, H., Langenberg, H., and Feser, F.: A Spectral Nudging Technique for Dynamical Downscaling Purposes, https://doi.org/10.1175/1520-0493(2000)128<3664:ASNTFD>2.0.CO;2, 2000.

Warner, T. T., Peterson, R. A., and Treadon, R. E.: A Tutorial on Lateral Boundary Conditions as a Basic and Potentially Serious Limitation to Regional Numerical Weather Prediction, Bulletin of the American Meteorological Society, 78, 2599–2617, https://doi.org/10.1175/1520-5 0477(1997)078<2599:ATOLBC>2.0.CO;2, 1997.

World Meteorological Organization: Guide to Climatological Practices, 3rd edition edn., http://www.wmo.int/pages/prog/wcp/ccl/ documents/WMO_100_en.pdf, 2011.

Wilby, L.R., and Fowler, J.H. 2011. regional climate downscaling. Available at: http://www.pages-perso-julie-carreau.univmontp2.fr/UM2/Packages_and_Tutorial_files/downscaling.pdf

Wei Wang, Cindy Bruyère, Michael Duda, Jimy Dudhia, Dave Gill, Michael Kavulich, Kelly Keene, Hui-Chuan Lin, John Michalakes, Syed Rizvi, Xin Zhang, Judith B Jonathan D. Beezley,

Janice L. Coen, and Jan Mandel erner and Kate Fossell, 2016 ARWUsersGuideV3pdf(http://www2.mmm.ucar.edu/wrf/users/docs/arw_v3.pdf).

Xiaoduo, P., Xin, L., Xiaokang, S., Xujun, H., Lihui, L., Liangxu, W. 2012. Dynamic downscaling of near-surface air temperature at the basin scale using WRF. Aacase study in the Heihe River Basin, China, *Front. Earth Sci*., 6(3), 314–323. doi: 10.1007/s11707-012-0306-2.

https://www.researchgate.net/profile/Luis_Martin_Pomares/publication/290946564_284_Solar_radiation_forecasting_with_WRF_model_in_the_Iberian_Peninsula/links/569cca5008ae879c64b652aa.pdf?

http://www.taccire.suanet.ac.tz/xmlui/bitstream/handle/123456789/472/Climate%20change%20and%20poverty%202006.pdf?sequence=1

http://www.nationsonline.org/oneworld/map/mali_map.htm

APPENDIX

Appendix A: Daily shortwave surface downward direct irradiance.

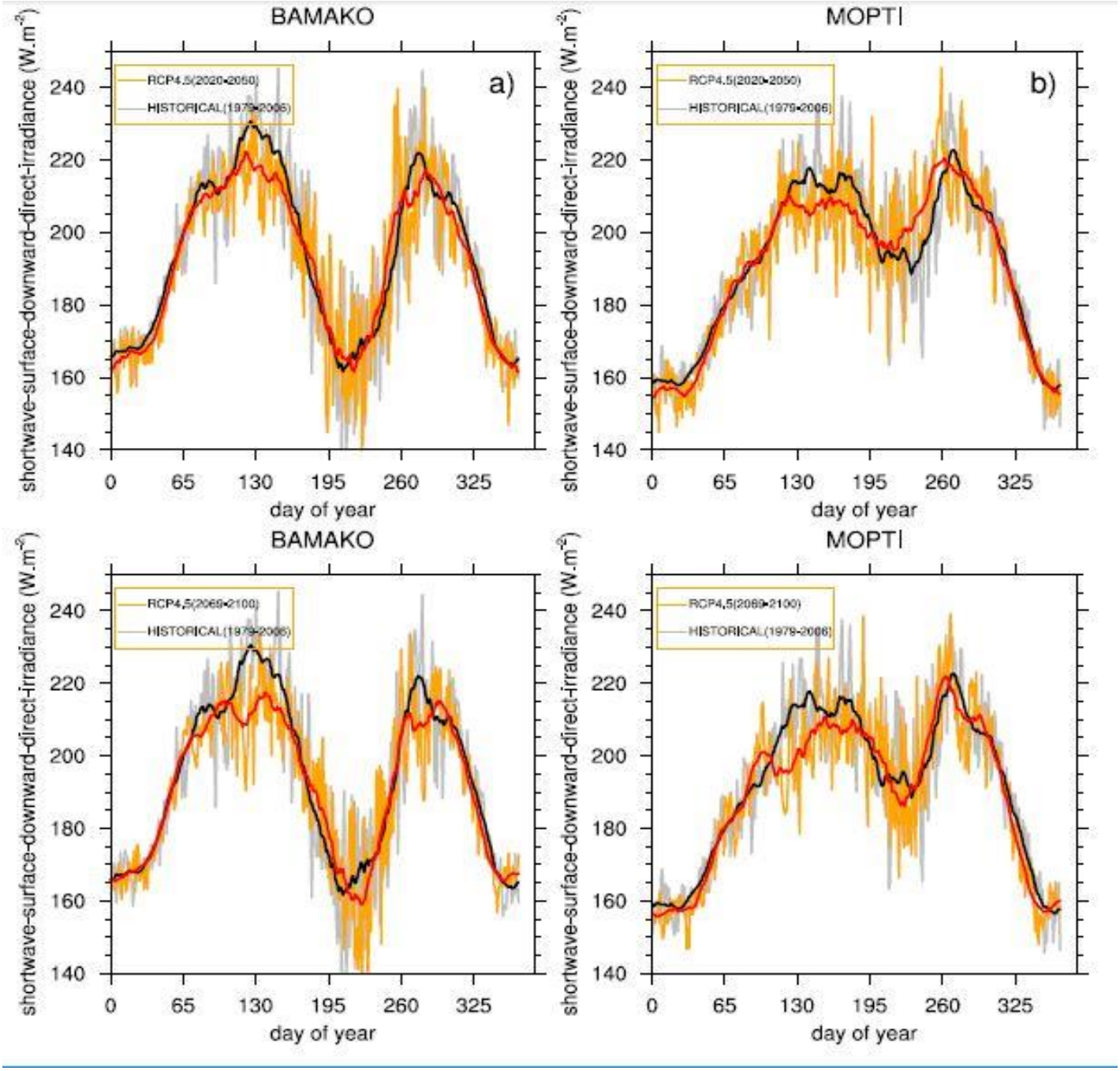

Figure 20:Daily shortwave surface downward direct irradiance

.

Appendix B: Daily shortwave surface downward diffuse irradiance.

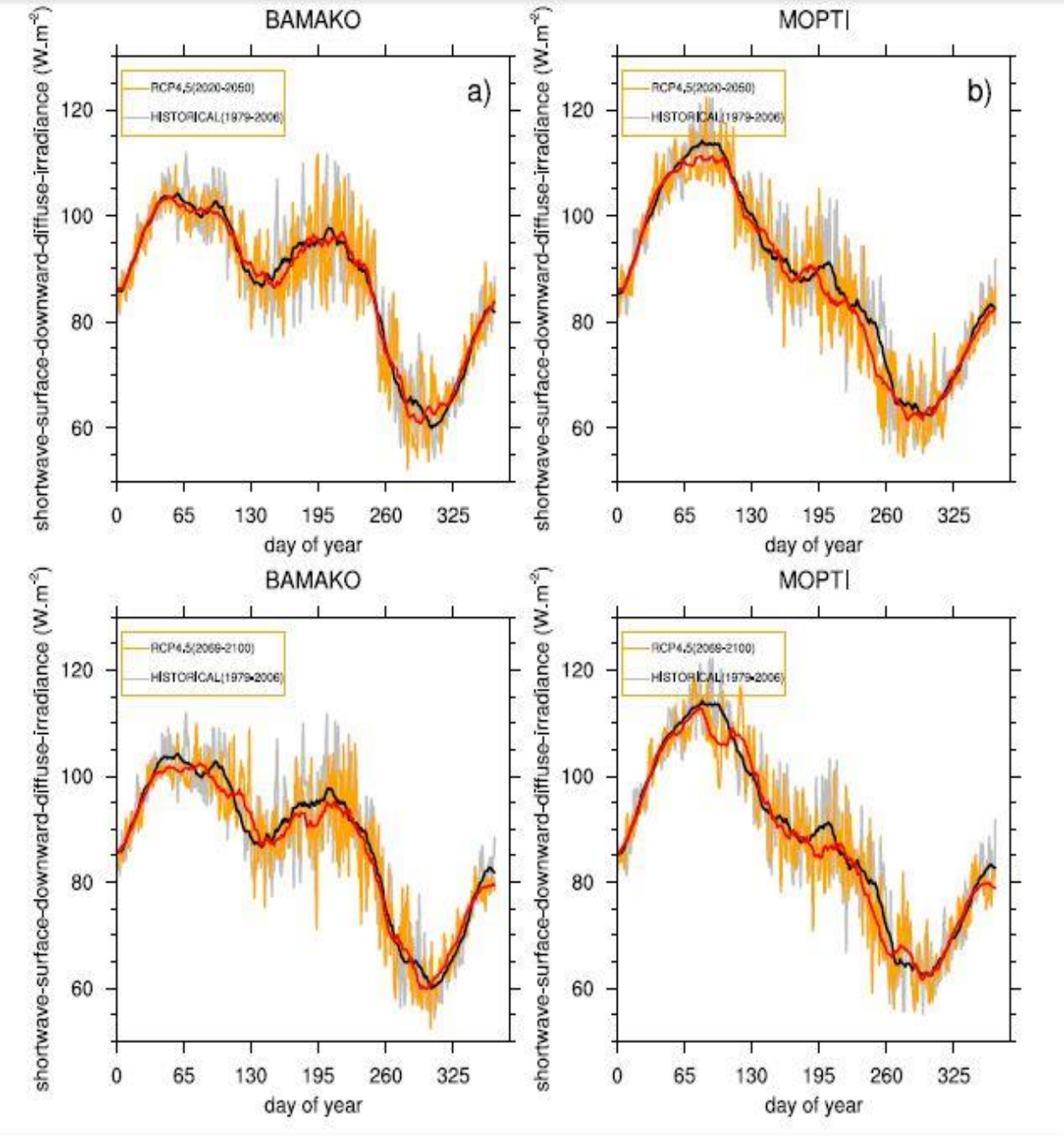

Figure 21:Daily shortwave surface downward diffuse irradiance.

Appendix C: Daily surface temperature.

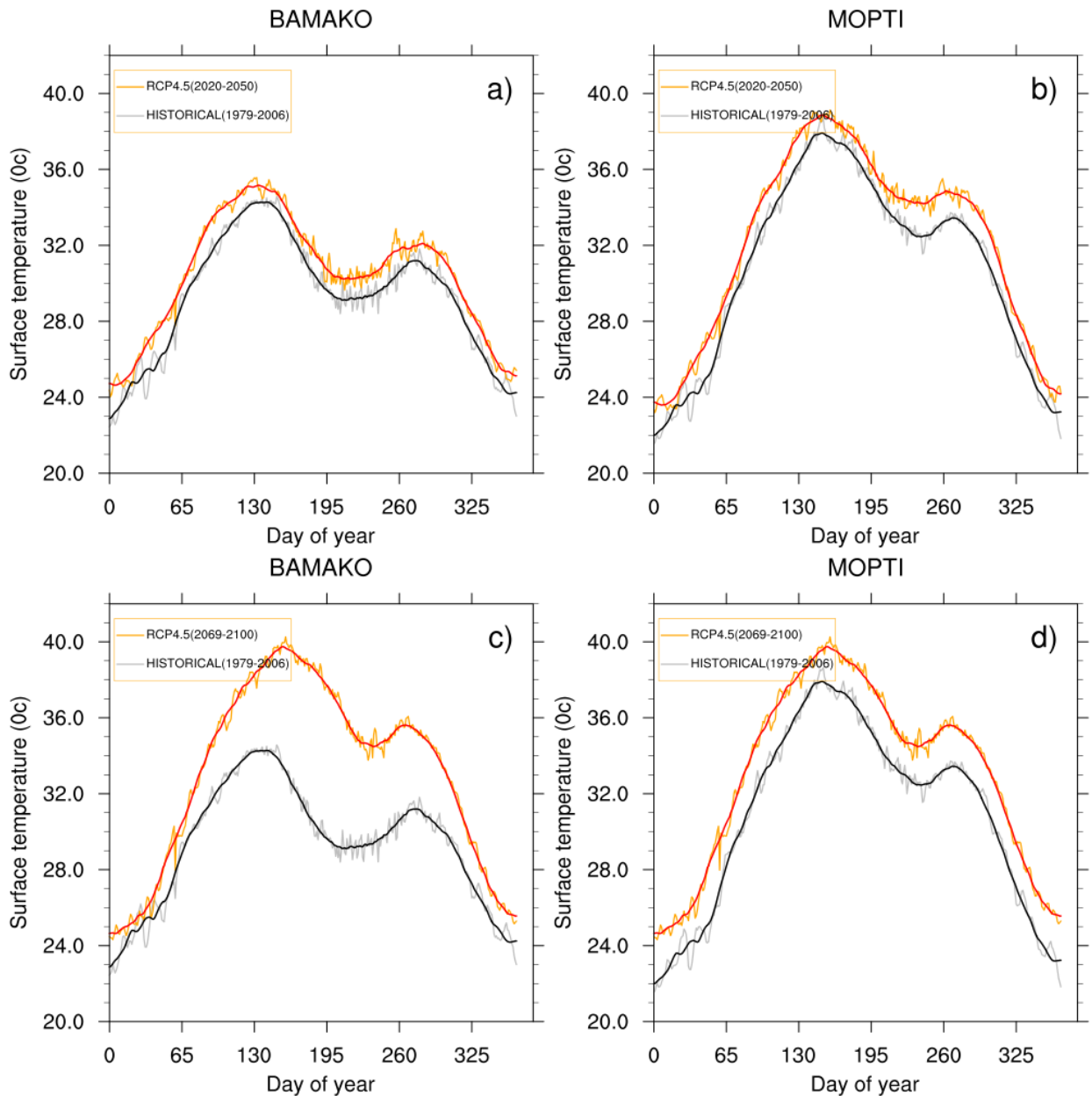

Figure 22:Daily surface temperature.